Accepted Manuscript

*Journal of the Geological Society*

# The erosional and weathering response to arc-continent collision in New Guinea

Peter D. Clift, Yifan Du, Mahyar Mohtadi, Katharina Pahnke, Mika Sutorius & Philipp Böning

DOI: https://doi.org/10.1144/jgs2023-207

To access the most recent version of this article, please click the DOI URL in the line above. When citing this article please include the above DOI.

Received 21 November 2023
Revised 6 March 2024
Accepted 26 March 2024



Supplementary material at https://doi.org/10.6084/m9.figshare.c.7168147

# The Erosional and Weathering Response to Arc-Continent Collision in New Guinea

Peter D. Clift[1,2]*, Yifan Du[1], Mahyar Mohtadi[3], Katharina Pahnke[4], Mika Sutorius[4], Philipp Böning[4]

1 Department of Earth Sciences, University College London, Gower Street, London, WC1E 6BT, UK

2 Department of Geology and Geophysics, Louisiana State University, Baton Rouge, LA 70803, USA

3 MARUM-Center for Marine Environmental Sciences, University of Bremen, 28359 Bremen, Germany

4 Institute for Chemistry and Biology of the Marine Environment (ICBM), University of Oldenburg, Carl-von-Ossietzky-Str. 9-11, 26129 Oldenburg, Germany

*Corresponding author: Peter D. Clift, Email: peter.clift@ucl.ac.uk

**Abstract:** Arc-continent collision is a fundamental stage in the plate tectonic cycle that allows the continental crust to grow and can influence global climate through chemical weathering. Collision between Australia and the oceanic North Coast Range-New Britain Arc began in the Middle Miocene resulting in uplift of the modern New Guinea Highlands. The temporal evolution of this collision and its erosional and weathering impacts is reconstructed here using sedimentary archives from the Gulf of Papua. Sr and Nd isotopes show dominant erosion from igneous arc-ophiolite crust, accounting for ~40–70% of the total flux in the Early Miocene, and rising to ~80–90% at 8 Ma, before falling again to 72–83% by the present day. Greater erosion from Australia-derived units accelerated in the Pliocene, like the classic Taiwan collision but with greater erosion from arc rather than continental units. Chemical alteration of the sediment increased through time, especially since ~5 Ma, consistent with increasing kaolinite indicative of more tropical weathering. Erosion was focused in the high topography where mafic arc units are preferentially exposed. Comparison of sediment with bedrock compositions implies that the source terrains have been more efficient at removing $CO_2$ from the atmosphere compared to Himalayan drainages.

*Keywords*: Erosion, weathering, climate, tectonics, geochemistry

Arc-continent collision is a key stage in the plate tectonic cycle and a critical way in which continent crust is built through the accretion of oceanic arc crust to continental margins (Clift *et al.* 2009b; Holbrook *et al.* 1999; Rudnick 1995). Oceanic arc collisions with passive continental margins represent one of the most common types of this process (Brown *et al.* 2011; Draut & Clift 2013; Scholl & von Huene 2010), the other being oceanic arc-active margin collisions. Collision between the Luzon Arc and Eurasia, forming the island of Taiwan represents a well-studied, albeit rather oblique example (Byrne *et al.* 2011; Huang *et al.* 2006; Suppe 1984). Here we examine the more orthogonal collision between the passive northern margin of Australia and the south-facing North Coast Range-New Britain Arc that has formed the mountains of New Guinea (Dewey & Bird 1970)(Fig. 1). We use relatively continuous marine sedimentary records from the Gulf of Papua to reconstruct the evolution in erosion patterns and chemical weathering since the onset of collision to understand the landscape response to the emergence of the island from the ocean. In Taiwan the colliding arc crust is largely accreted, although the great majority of the Taiwan mountains are formed from offscraped Chinese passive margin sediments, with the accreted arc crust present at depth (Clift *et al.* 2009a; Hsieh & Yen 2016; Wu *et al.* 2014). In contrast, in New Guinea the presence of ophiolite and arc igneous rocks exposed in the Highlands (Davies & Jaques 1984; Davies 2012) suggests a different style of collision and potentially contrasting ability to preserve the arc crust.

## Chemical Weathering

Understanding the process of tectonic accretion in New Guinea, and the subsequent erosion is also important because of its potential impact on the chemical weathering flux in Southeast Asia. Silicate weathering is recognized as being critical to removing greenhouse $CO_2$ gas from the atmosphere, and so balancing $CO_2$ supplied by mantle degassing during magmatism. By doing so weathering is believed to keep the Earth's climate in a relative steady state condition (Berner & Berner 1997; Kasting 2019; Penman *et al.* 2020). Breakdown of silicate minerals results in consumption of atmospheric $CO_2$, the most critical greenhouse gas over timescales of $>10^3$ y. Although initial attempts to understand how mountain building during the Cenozoic may have affected global cooling since the Eocene mostly invoked erosion of the Himalaya and Tibetan Plateau (Raymo & Ruddiman 1992;

Raymo *et al.* 1988), it now seems that weathering fluxes in that region have decreased during the Neogene as global average temperatures reduced (Clift & Jonell 2021). Furthermore, lithium isotopic evidence indicates steady-state global silicate weathering flux during the Cenozoic that also argues against the importance of Himalayan erosion (Caves *et al.* 2016). Instead, greater reactivity (weatherability) of bedrock during the Cenozoic has been advanced as an alternative to reconcile the stable weathering flux with the evidence for decreasing atmospheric $CO_2$. Greater weatherability might be achieved by either increasing the availability of fresh minerals through faster erosion and/or an increase in the supply of reactive minerals (Caves Rugenstein *et al.* 2019).

The role of tropical, magmatic arc units has been invoked as a critical part of the climate control system (Jagoutz *et al.* 2016; Macdonald *et al.* 2019) because these may account for the greater weatherability. Their mafic composition results in more $CO_2$ consumption during chemical weathering compared to sources with typical continental compositions (Caves Rugenstein *et al.* 2019; Hartmann *et al.* 2014). When these systems are in tropical regions with relatively high temperatures and high humidity then the rate of chemical weathering may be high (West *et al.* 2005). Recent studies have highlighted the potential of the islands offshore SE Asia as being important to global weathering fluxes since 4 Ma (Bayon *et al.* 2023; Martin *et al.* 2023; Park *et al.* 2020), yet the evolving history of this weathering has yet to be revealed.

While we examine the evidence for silicate weathering of New Guinea in this study, we do not do so in ignorance of other weathering feedbacks that may affect the net impact on $CO_2$. The consumption of $CO_2$ by silicate weathering can be offset by $CO_2$ release caused by chemical weathering of carbonates. Weathering of pyrites in shales forms sulfuric acid that can then react with limestones and release $CO_2$ to the atmosphere (Calmels *et al.* 2007; Li *et al.* 2008; Torres *et al.* 2014). Nonetheless, geochemical modelling of sulfide weathering has highlighted the feedbacks on atmospheric oxygen associated with the organic carbon cycle. An increase of sulfide weathering may lead to $CO_2$ release but is then followed by a greater sink of $CO_2$ (Maffre *et al.* 2021). Limestone units are exposed in the New Guinea Fold and Thrust Belt (Fig. 1) and these account for ~15% of the land area that now drains into the Gulf of Papua (Table 1), meaning that this may be significant but likely subsidiary to the silicate weathering, given the relative extent of the outcrop. Correcting for this process is not possible using evidence from the marine sedimentary record because dissolution leaves no residue that might be preserved and then measured.

Another potential source of $CO_2$ release is the oxidation of organic carbon preserved in older sedimentary rocks. This process could also release $CO_2$ back to the atmosphere (Hilton *et al.* 2021). Faster physical erosion has been linked to higher rates of rock organic carbon oxidation. However, in the example of Taiwan the generation of $CO_2$ by this method was outstripped by the sequestration of $CO_2$ via organic carbon burial offshore (Hilton *et al.* 2014). This may also be a factor in New Guinea where the sediments deposited close to the coast shows high organic carbon contents (>1%) (Rosenthal *et al.* 2018).

Weathering of rock organic carbon is estimated to approximate or even exceed $CO_2$ drawdown caused by silicate weathering in several high and actively uplifting mountain belts (Zondervan *et al.* 2023). Studies of Taiwan indicate that when erosion is fast, then carbonate and sulfide weathering tends to dominate and net $CO_2$ is released (Bufe *et al.* 2021). However, in lower-lying areas where uplift is slow or absent, erosion is also slow and silicate weathering can dominate (Bufe *et al.* 2021). This is especially true on flood plains where sediment may be stored for long periods prior to final delivery to a marine depocentre (Bouchez *et al.* 2012; Lupker *et al.* 2012; Repasch *et al.* 2021). In New Guinea there is a mixture of catchment types. Rivers in the eastern Papuan Peninsula have relatively restricted coastal flood plains, but in the west the Fly River and its tributaries have lengthy flood plains where chemical weathering may be important. In this study, we focus on reconstructing trends in silicate chemical weathering through time and do not attempt to budget the organic carbon cycle.

## Geological Setting

Initial collision between Australia and the North Coast Range-New Britain Arc dates back to the Oligocene. Evidence for deformation of that age is seen in the eastern Papuan Peninsula (Baldwin *et al.* 2012)(Fig. 1A). Metamorphism and magmatism in the Bird's Neck region of NW New Guinea also testifies to an Oligocene collision, following a period of oblique subduction of the Australian plate under the Philippine Sea Plate (Webb *et al.* 2020). In the eastern Papuan Peninsula the Papuan Ultramafic Belt is composed of mantle peridotites, gabbros and basalts which overthrusts felsic crust affiliated with the Australia continental margin, forming the Kagi and Emo Metamorphic Complexes that are exposed within the Owen Stanley Range (Davies & Smith 1971; Lus *et al.* 2004). Subduction polarity reversal followed the Oligocene collision resulted in eruption of a 18–12 Ma suite of volcanic rocks linked to underthrusting of the Philippine Sea Plate beneath the Australian Plate, prior to final collision (Webb *et al.* 2020).

New Guinea has experienced significant tectonically driven rock uplift, especially in the last 12 m.y., when the Australian Plate began to finally collide with the North Coast Range-New Britain magmatic arcs in the Central Highlands region (Davies 2012; van Ufford & Cloos 2005). Middle-Upper Miocene sedimentary rocks (Koor Formation) in NW New Guinea are folded and were followed by a hiatus ~10.5–4.5 Ma that is interpreted to indicate collision between Australia and the North Coast Range-New Britain Arc (Webb *et al.* 2019). Volcanic rocks of the Maramuni Arc that are exposed in the eastern Highlands span 12–6 Ma and show a geochemical evolution of increasing recycling of Australian crust through the roots of the arc starting at 9 Ma, after initial collision with the trench at 12 Ma (Holm *et al.* 2015). A further change at ~7 Ma implies breakoff of the Australian slab at that time. Recent reconstructions of the Central Highlands based on structural analysis and thermochronology indicate rapid exhumation between 10 and 6 Ma that is believed to reflect erosion in response to rock uplift starting ~10 Ma (Martin *et al.* 2023).

The mountains of the Central Highlands comprise accreted arc units, including the Sepik Complex of volcanic and intrusive mafic and ultramafic rocks and associated sedimentary rocks, interpreted to represent an accreted magmatic arc unit (Brown *et al.* 1979; Davies 2012; Klootwijk *et al.* 2003) (Fig. 1B). The Maramuni Arc and the Papuan Ultramafic Belt are both major tectonic units composed of ultramafic mantle, layered gabbro and basaltic rocks (Davies & Jaques 1984). Further mafic oceanic basalts are found at the eastern end of the Papuan Peninsula, where a weakly deformed 1-km-thick sequence of Eocene basalts is intruded by minor Mid Miocene shoshonite volcanic rocks (Smith & Davies 1976).

South of the arc units there is an accretionary prism that formed prior to and during collision. This is now preserved south of the Finisterre Mountains (Abbott *et al.* 1994a). A change in provenance from purely volcaniclastic to a mixed volcaniclastic-siliciclastic assemblage in the accretionary prism sediments has been interpreted to indicate the start of collision with continental Australia ~16–18 Ma (Abbott *et al.* 1994b). Further south the Aure Accretionary Prism comprises Upper Oligocene-Miocene and Pliocene, largely siliciclastic sedimentary rocks (Dow *et al.* 1974). Further east, along the southern coast of the Papuan Peninsula the Aure Complex transitions into an Eocene-Oligocene, pre-collisional accretionary prism built from Paleocene-Eocene siliciclastic sedimentary rocks, with lesser volumes of serpentinite (Fig. 1B). This sequence has been intruded by Oligocene gabbro and the whole assemblage was metamorphosed to lower greenschist facies (Davies 2012).

The final stages of collision between a north-dipping Australian continent and the North Coast Range-New Britain Arc started in the Early Miocene, when units of the Australian margin were subducted and metamorphosed before being imbricated into a thrust stack (Baldwin *et al.* 2012; Cloos *et al.* 2005; Holm *et al.* 2015). Continued convergence resulted in progressive emergence of a landmass that is estimated to have started as a small island after 15 Ma but that had extended to a feature >500 km long by 12 Ma, when rapid exhumation began (Martin *et al.* 2023). This island now spans 2600 km in length. Syn-collisional delamination of the underthrusting Australian slab was the primary driver for significant surface uplift of ~2.5 km starting in the Late Miocene, with further uplift linked to the Pliocene rifting of the Woodlark Basin (Little *et al.* 2007; Taylor *et al.* 1995).

Sediment eroded from the New Guinea Highlands and that is transported towards the west is delivered to the Timor Trench, where it is subducted or offscraped into an accretionary prism (Harris 2011). As a result, reconstructing the history of erosion using sediments from that area is difficult or impossible. In contrast, sediment transported towards the east of the collision zone enters the Gulf of Papua, which opened by rifting of continental blocks from Australia during the Cretaceous and seafloor spreading in the Paleocene (Bulois *et al.* 2018; Weissel & Watts 1979).

New Guinea is a hotspot of modern erosion, linked in part to the high annual precipitation (McAlpine *et al.* 1983). The Highlands are eroding quickly, reflected in the 115 Mt/y of sediment carried by the Fly River in pre-industrial times (Milliman & Syvitski 1992). Other rivers on the Papuan Peninsula also supply significant sediment to the gulf, including the Purari and Aure Rivers, with loads of 80 and 50 Mt/y respectively (Milliman & Syvitski 1992). The Papuan Peninsular rivers largely drain the Owen Stanley Metamorphic Complex and the Aure Accretionary Prism. Despite this potential the weathering flux from New Guinea has yet to be estimated through geological time. At present New Guinea is estimated to contribute ~44% of the weathering flux from SE Asia, estimated at 0.27 Tmol/yr from analysis of the water chemistry (~5% of the global flux) (Dessert *et al.* 2003; Hartmann *et al.* 2009; Hartmann *et al.* 2014; Park *et al.* 2020). Its longer-term influence is preserved in the marine sediment record.

Although some of the sediment is captured in the proximal foreland basin developed south of the New Guinea Highlands (Dalrymple *et al.* 2003), sediment from the Fly River forms a thick Plio-Pleistocene delta sequence that overlies an older carbonate platform (Pigram *et al.* 1989; Tcherepanov *et al.* 2010). In contrast, the deep-water sediment in the Gulf of Papua holds a fine-grained sedimentary record spanning the collision of Australia

with the North Coast Range-New Britain Arc since the Early Miocene. This sequence was sampled by scientific drilling in the early 1970s (Shipboard Scientific Party 1973, 1975), and although the recovery was in the form of partial "spot" coring this provides a low-resolution, long duration record of the evolving provenance and chemical weathering of the source regions.

## Sampling

150 samples of muddy siltstone were taken from cores recovered at Deep Sea Drilling Project (DSDP) Sites 210 and 287, located ~1200 km from the mouth of the Fly River in the deep-water Gulf of Papua (Fig. 1A). Because the basin ceased seafloor spreading in the Paleocene (Bulois *et al.* 2018; Weissel & Watts 1979) the distance between the drill sites and the Australian crust in New Guinea and mainland Australia has remained constant since that time. The rifted pieces of Australia crust moved north relative to the mainland prior to the Eocene but did not move relative to the drill sites during the time considered here. Site 210 has the most expanded stratigraphy and penetrated >720 m below sea floor (mbsf) into Eocene carbonates (Fig. 2). In contrast, the Miocene is largely missing at Site 287, which recovered basaltic basement at ~240 mbsf. Age control is based on a matrix of nannofossil and foraminiferal assemblages (Shipboard Scientific Party 1973, 1975). A numerical age was assigned based on the time scale of Gradstein *et al.* (2020), with depositional ages of individual samples calculated assuming linear sedimentation rates between control points.

## Methodology

The samples were analysed for grain size, major and trace element geochemistry, Sr and Nd isotope composition and clay mineralogy to constrain the provenance and changing intensity of chemical alteration of sediment supplied from New Guinea. These proxies were chosen because of their previous effectiveness when applied to similar sections in this and surrounding regions (Clift *et al.* 2014; Peng *et al.* 2021). Complete details concerning analytical conditions are provided in the Supplementary Information files.

### *Grain size Analysis*

For quantitative grain size analysis, samples were prepared using standard procedures (Hülse & Bentley 2012) and analysis was conducted on a Beckmann Coulter LS13 320 laser diffraction particle size analyser at Louisiana State University (LSU). Results are provided in Table S1.

*Major and Trace Element Analysis*

Analysis for major element compositions of the bulk sediment was carried out using the Bruker S2-PUMA energy-dispersive X-ray fluorescence (XRF) instrument in the Chevron Geomaterials Characterization Laboratory (CGCL) in the Department of Geology & Geophysics at LSU. Selected major and trace elements were also measured by XRF using a benchtop ED-XRF spectrometer at MARUM, University of Bremen. Results are provided in Table S2, with data from repeat analyses of standards in Table S3. Major element ratios were calculated from the conventional XRF results, with the benchtop data being used for trace elements compositions and ratios

*Radiogenic Isotope Analysis*

Bulk decarbonated sediment Sr and Nd isotopes were used to constrain the provenance of the sediment, which is a critical factor in assessing chemical weathering because the initial source composition is a major control on sediment chemistry. The isotopic compositions of Nd and Sr were analysed on a Thermo Scientific Neptune Plus Multicollector ICP-MS at the ICBM, Oldenburg, Germany. The Nd isotopic composition is expressed in $\varepsilon_{Nd}$ notation, using the Chondritic Uniform Reservoir with a value of 0.512638 (Jacobsen & Wasserburg 1980). Results are reported in Table 2.

*Clay Mineralogy*

Clay mineralogy measurements were undertaken using a PANalytical Empyrean X-Ray Diffractometer at LSU. The semi-quantitative method of Biscaye (1965) was used to estimate the clay assemblage, which is based on peak-intensity factors determined from calculated XRD patterns, as measured by MACDIFF software. Results are provided in Table S4.

**Results**

*Grain size*

Grain size analyses confirm that the sediment is dominantly composed of very fine silt (Fig. 2) and progressively fining up-section at Site 210 from the Mid Miocene to the Upper Pleistocene, followed by a trend to coarser sediment in the top 40 m. Likewise, sediments from Site 287 show a slight coarsening trend between the Pliocene and the Recent. When plotted against depositional age the temporal evolution in grain size is seen to be

similar at both sites, with a mean close to $\phi = 6$ (medium silt) since ~17 Ma until 8 Ma, followed by fining to $\phi = 8$ (very fine silt) until 1–2 Ma (Fig. 3A). We further consider sediment kurtosis, a measure of how distributed the grain size spectrum is for each sample, i.e., sorting. Again, there is a modest amount of variability, with a rise in kurtosis recorded from 17 Ma until 1–2 Ma (Fig. 3B). This implies that the sediment became slightly better sorted through time.

The very limited range of grain sizes in the studied sediments makes it unlikely that this factor controlled any of the proxy records presented. We test this assumption by plotting Chemical Index of Alteration (CIA)(Nesbitt *et al.* 1980) against mean grain size (Fig. 4A). This proxy is based on the relative loss of water-mobile Ca, K and Na relative to immobile Al during chemical weathering. Although developed for soils this proxy has been widely applied to marine sediments. The Ca is only that related to silicate minerals and not biogenic carbonate-based Ca. The plot shows a poorly defined positive correlation, with a low correlation coefficient ($R^2 = 0.2339$). Under normal circumstances smaller grains would be expected to be more altered than larger ones, and our data is consistent with this relationship. If we consider Mg/Al as a weathering proxy because it is potentially more relevant to chemical weathering in a region with a high density of mafic (i.e., Mg-rich) source rocks, then we see a slightly improved but still relatively poor correlation ($R^2 = 0.3175$) (Fig. 4B).

*Major and Trace Element Geochemistry*

The general chemical character of the sediments can be assessed using simple discrimination diagrams. The triangular CN-A-K diagram of Fedo *et al.* (1995) based on molar percentages of CaO, $Na_2O$, $K_2O$ and $Al_2O_3$ shows that the sediments form a single array stretching from close to the CaO+$Na_2O$ end member towards the upper end of the compositional range of illite (Fig. 5A). This indicates that the sediments represent a range of alteration products formed by the progressive breakdown of pristine minerals and the formation of illite ± kaolinite. It is noteworthy that sediments indicate a large range in CIA, shown in the y-axis of this plot. CIA values close to 50 imply relatively fresh material, while at the high-end values of ~80 indicate strong chemical alteration. The data can also be plotted on the discrimination diagram of Herron (1988)(Fig. 5B). The samples form a tight grouping, largely within the Fe Shale field, with some overlap into the Shale field. This demonstrates the limited range in the bulk sediment geochemistry of the samples, reflecting the restricted grain size.

Temporal trends in chemical alteration can be tracked using the ratio of water-mobile versus immobile elements. K is common in K-feldspars and biotite micas and is more readily mobilized than Al, making K/Al a common alteration proxy. Although K/Al may also be affected by grain size the range here is so small that this issue may be safely ignored (Lupker *et al.* 2012). The temporal trend in K/Al shows a poorly defined trend to slightly lower values from the Early Miocene until ~8 Ma followed by a rise and then a well-defined trend to lower values starting after ~5 Ma (Fig. 6D). If source composition remained relatively constant then such trends would indicate changes in chemical alteration, and especially a trend to more alteration since 5 Ma. Different combinations of mobile versus immobile ratios allow us to track alteration for different source rocks, with contrasting mineralogy and bulk chemistry. Unsurprisingly, Na/Al shows a similar trend another because Na is a similar but more mobile alkali element (Fig. 6F). Because Na is common in seawater and might be enriched in marine sediments the similarity with K/Al is reassuring.

Rb is found in K-feldspars, micas and clays and although more mobile than Al it is less mobile than K (Heier & Billings 1970). Studies of sediment from South China Sea demonstrated that K/Rb is sometimes a more sensitive weathering proxy than K/Al (Hu *et al.* 2016). K/Rb values show a regular fall in values through the section from ~240 at 23 Ma to 220 at 7 Ma, and with a well-defined later fall to ~175 by the Recent (Fig. 6E). The apparent rise in K/Al values between 8 and 5 Ma is not seen in the K/Rb record. We further consider Mg and Ca, as being elements preferentially leached from silicate minerals during alteration. Mg is rich in the mafic source rocks that outcrop in the New Guinea Highlands. Like K/Rb, Mg/Al shows a long-term decline, especially after 5 Ma (Fig. 6G). Ca/Al also reduced with time, but this trend is the least dramatic or well defined (Fig. 6H).

These weathering proxies can be further compared with the CIA (Fig. 6C). Again, there is a poorly defined, relatively decreasing trend from 23 Ma to ~7 Ma, where there is a minimum, followed by a progressive trend to higher values, especially from 6 to 3 Ma. The CIA record is generally noisier than seen in K/Al, and especially Mg/Al. Following the weathering study of Peng *et al.* (2021) that targeted cores from offshore northern New Guinea, we also consider two other weathering proxies. CIX is the same as CIA but excludes calcium (CIX = CIA eXcluding Ca), and thus the potential for contamination from biogenic carbonate (Garzanti *et al.* 2014). CIX is stable through time from 23 and to 5 Ma and then shows a rise, indicating more chemical alteration from that time to the present (Fig. 6B). The trend is less noisy than that defined by regular CIA. Finally, the Index of Compositional Variability (ICV) is defined as the ratio of $CaO^* + K_2O + Na_2O + Fe_2O_3 + MgO + MnO +$

$TiO_2$ relative to $Al_2O_3$ (Cox *et al.* 1995)( CaO* is Ca related to silicate minerals only). Like many of the other proxies the temporal trend is for stability from 23 to 5 Ma, followed by falling values and thus more alteration after 5 Ma (Fig. 6A).

Because the state of chemical weathering may be related to the duration of transport and residence in floodplains rather than the rate of chemical weathering, we also look at a select number of these weathering proxies normalised against the sedimentation rate. Figure 7A shows the trend in the CIA which is generally low until ~8 Ma and then accelerated after 6 Ma to scattered but often high values during the Plio-Pleistocene. Similar patterns are also seen in the CIX (Fig. 7B) as well as Mg/Al (Fig. 7C) and K/Al (Fig. 7D). The normalising procedure emphasises the significant increase in chemical weathering seen in the New Guinea sediments since 6 Ma.

We further consider elements that are more closely tied to the provenance of the sediment and especially tracers that might quantify the competing influence of the colliding arc and the offscraped Australian continent. Zr concentration is largely a reflection of zircon abundance. This mineral is most common in felsic igneous rocks and in siliciclastic sedimentary rocks but is less common in mafic rocks. Zirconium might be expected to rise with greater erosion from continental rocks. There is a well-defined trend to higher Zr concentrations through time, rising from ~100 ppm at 23 Ma to ~140 ppm by Recent times (Fig. 8A). The trend is especially pronounced since 5 Ma. Titanium is rich in rutile and ilmenite, which are found in high grade metamorphic rocks and intrusive igneous rocks (Zack & Kooijman 2017). Ilmenite is especially associated with cumulate igneous intrusions (Anthony *et al.* 2022), although it is not exclusive to felsic or mafic rocks. The concentration of Ti increases gradually through time, especially after 5 Ma and mirrors the trend in Zr (Fig. 8B). Chromium is primarily found in chromite, which in turn is associated with mafic and ultramafic intrusions, as well as in pods within the mantle (Dawson & Smith 1975; Lorand & Ceuleneer 1989), so that it might be associated with erosion of the ophiolite and arc lower crustal rocks. Chromium contents in the DSDP sediments however show no temporal evolution (Fig. 8C). Nickel is found mostly in laterite soils (Gleeson *et al.* 2003), formed by weathering of mafic igneous rocks, where it is concentrated in limonite and garnierite. Ni-rich laterites are common weathering products of peridotite (Golightly 1981). The temporal evolution in Ni (Fig. 8D) shows a rapid drop in values from 23 to 16 Ma, followed by a more gradual long-term decrease from that time until the present.

*Nd and Sr Isotopes*

Radiogenic isotopes have a long history as being effective provenance proxies, especially for resolving between erosion of ancient continental crust and primitive arc or oceanic rocks (Garçon *et al.* 2014; Jonell *et al.* 2018). The Sr and Nd isotopic composition of sediments from Site 210 shows coherent long-term trends (Figs. 8E and 8F). The $^{87}Sr/^{86}Sr$ values were variable before ~7 Ma, with a long-term moderate decrease between 23 and 7 Ma. After 7 Ma the $^{87}Sr/^{86}Sr$ values were more variable, but also trend to higher values. $\varepsilon_{Nd}$ values show coherent variation (Fig. 8F). From 23 until 14 Ma $^{87}Sr/^{86}Sr$ values increased followed by a period of relative stability from 14 until 8 Ma. Subsequently values fell until the present day, although again there was significant variability after 5 Ma (Figs. 8E). $\varepsilon_{Nd}$ values reflect the average age that the source rocks have been in the crust after separation from the upper mantle source (DePaolo & Wasserburg 1976), so that higher $\varepsilon_{Nd}$ values reflect more primitive, younger rocks. $\varepsilon_{Nd}$ values are seen to rise from the Early Miocene, reaching a peak in the Middle Miocene around 14 Ma. $\varepsilon_{Nd}$ values then remain relatively constant until around 8 Ma and then progressively declined to the present day, although becoming more variable after 5 Ma, with some especially low $\varepsilon_{Nd}$ values recorded in the Pliocene and Pleistocene (Fig. 8F).

*Clay Minerals*

Clay minerals can be used as indicators of weathering environments (Thiry 2000), and under certain circumstances as provenance proxies (Liu *et al.* 2007). This approach assumes no major change due to burial diagenesis. Heat flow in the deep-water Gulf of Papua is estimated at ~60 $mW/m^2$ based on the age of the oceanic crust (Stein & Stein 1992), equivalent to a geothermal gradient of ~43 °C/km. Since the deepest sample considered here was taken at 520 m below seafloor this implies peak temperatures of ~22 °C, insufficient to have caused significant diagenesis. Kaolinite contents show a trend to greater percentages starting in the Early Miocene (Fig. 9A), although in the Middle and Late Miocene there was a lot of short-term variability. There is a significant increase in kaolinite at ~14 Ma. Although the record is rather noisy, there was a fall to lower values at around 5 Ma. Between 5 Ma and the present there was a constant increase in kaolinite percentages from ~10% to ~18%. As a mirror to this, the contribution that smectite plays within the total clay assembly shows the opposite trend, especially after 5 Ma, with a long-term drop in the content from >80% in the Early Miocene to <60% in recent times (Fig. 9B). The fall in smectite abundance is poorly defined between the Early Miocene and Late Miocene although again, an increase just before

5 Ma is clearer, as is the fall after that time (Fig. 9C). Smectite/(illite + chlorite) is a commonly used proxy (Colin *et al.* 1999) that shows the intensity of chemical weathering compared to physical weathering/erosion. In this case, there is a long-term fall in values, indicating less chemical weathering under a seasonal climate after 5 Ma and more physical erosion. (Fig. 9B). Likewise, the ratio between smectite and kaolinite can be used to assess the relative importance of seasonal versus tropical weathering (Alizai *et al.* 2012)(Fig. 9D). The downward trend in this ratio through the time studied here indicates relatively less seasonal weathering and more tropical conditions with a particularly well-defined reduction starting ~5 Ma after a sharp rise from a minimum just prior to that time.

## Discussion

### *Chemical Weathering History*

Considering the preferred proxies for chemical alteration, these show many of the same temporal trends (Fig. 6). There is a minimum in chemical alteration at 5–7 Ma according to K/Al and Na/Al, although many of the other proxies do not show much coherent variability prior to that time, especially when normalized to sedimentation rate (Fig. 7). At each site the maximum sedimentation rate was set to a value of 1 and the measured proxy was then multiplied by the normalized sedimentation rate before being normalized again within the range of values measured in the original proxy. Before ~7 Ma, chemical weathering intensity appears to have been relatively constant since 23 Ma according to many of the other proxies, including ICV, CIA and Mg/Al. Because of the low data density before ~7 Ma it is hard to have great confidence in any trend. The clearest signal observed is a trend starting from 5–7 Ma until the present day showing progressively more intense chemical alteration of the sediments, a trend that correlates with falling global average temperatures (Fig. 10E). It is noteworthy that the trend to greater alteration is the opposite of that seen in the Asian marginal seas, where alteration is less intense in more recent times (Clift & Jonell 2021; Wan *et al.* 2007; Zhou *et al.* 2021). The increasing alteration could be a reflection of faster rates of chemical weathering or more time spent by sediment in the weathering zone, most notably in flood plains that would be expected to prograde and increase with time.

An increase in alteration might be anticipated to result in an increase in those clay minerals produced by chemical weathering, and indeed the proportion of kaolinite did increase, especially after 5 Ma (Fig. 9A, 10B). Kaolinite is particularly favoured by tropical weathering in hot, humid conditions (Hillier 1995). In contrast, the proportion of smectite in

the sediment fell through time (Fig. 9B), indicating that decreasing smectite is not simply a response to weaker chemical weathering but may be linked to change in weathering type. The increasing proportions of kaolinite likely indicate greater tropical weathering, consistent with the northward motion of Australia during the Neogene (Cohen *et al.* 2013; Hall 2002).

Several studies have linked the formation of smectite to the chemical weathering of volcanic rocks (Tomita *et al.* 1993), and if this is a factor, this would also imply that the proportion of volcanic rock in the sources reduced since the Early Miocene, an interpretation that is in accord with the rising Zr contents and falling $\varepsilon_{Nd}$ values (Fig. 8A, 8F), although only after ~5 Ma. Falling smectite before 5 Ma occurred in the context of rising $\varepsilon_{Nd}$ values that suggest more, not less, volcanic input, and indicating that environmental factors were more important prior to 5 Ma in controlling clay mineralogy. Likewise, the smectite/(illite + chlorite) should reflect the importance of chemical weathering in a seasonal climate (Colin *et al.* 1999). This proxy shows a lot of scatter and little coherent trend (Fig. 9C). If we just consider a long-term average, then a decrease in this proxy can be seen largely mirroring the trend shown in the total smectite contribution.

The falling abundance of smectite through time may indicate that the seasonality of the environment was reducing, as would be expected as the setting became more tropical during Australia's northward drift (Metcalfe 2013). Together with the geochemical evidence (Fig. 6), the clay minerals are supportive of stronger chemical weathering since the Early Miocene but especially since the start of the Pliocene, ~5 Ma. This alteration must have occurred under tropical conditions.

*Provenance Evolution*

The increase in Zr through time (Fig. 8A and 10C) implies progressively greater erosion of continental crust, starting ~5–7 Ma. This erosion mirrors the ongoing imbrication of slices of Australian continental crust into the Fold and Thrust Belt (Baldwin *et al.* 2012; Craig & Warvakai 2009) and their exhumation (Martin *et al.* 2023). This is the largest expanse of exposed continental material in New Guinea so that the progressive uplift of these units might be anticipated to result in a gradually increasing erosional signal as the uplifting thrust sheets are incised by rivers. Earlier topographic growth appears to have mostly involved the colliding arc rocks. Chromium is typically associated with chromite (spinel) contents abundant in mantle peridotite rocks and in mafic layered intrusions. As a result, Cr could serve as a proxy for erosion from the New Guinea Mobile Belt or Papuan Ophiolites.

However, apart from having a sparse array of low Cr values at 2–3 Ma and 16–17 Ma (Fig. 8C) there is little temporal trend in Cr content. Our analysis may indicate a consistent and long-lived erosion from deep crust and oceanic mantle rocks from within the accreted arc and ophiolites into the Gulf of Papua since the Middle Miocene.

The temporal evolution in Ni (Fig. 8D), a proxy for the erosion of laterites or ultramafic cumulates in ophiolite complexes (Lorand & Ceuleneer 1989; Page 1986), favours the strongest rate of laterite recycling during the Early Miocene, followed by a marked decrease. Volcanic arc rocks in tropical settings are prone to intense chemical weathering and laterite formation, which would then be eroded as the arc was uplifted during initial collision. The early decrease in Ni is interpreted to indicate that laterites dominated erosion prior to and during early collision and that stronger physical erosion dominated as the collision progressed. Active rock uplift reduces the opportunity to form soils which require tectonic stability and long periods of time and dilutes any laterite-derived sediments with newly eroded material.

Neodymium isotopes provide important additional constraints on provenance evolution. The general increase in $\varepsilon_{Nd}$ values from 23 until 14 Ma (Fig. 8F) indicates greater erosion from primitive arc crust rather than the Australian continent. This trend precedes the generally accepted age for the start of collision (Baldwin *et al.* 2012; van Ufford & Cloos 2005) and implies that island arc units had already been uplifted and eroded prior to the final collision between the North Coast Range-New Britain Arc and Australia. The reverse trend began after ~7 Ma and especially after 5 Ma, at the onset of hard collision, and implies increasing degrees of erosion from accreted Australian crust, which were being unroofed by that time (Martin *et al.* 2023). Nonetheless, the generally high $\varepsilon_{Nd}$ values would suggest that erosion from offscraped Australian units must be relatively modest for much of the history. The Sr isotopes are consistent with this interpretation. The occurrence of scattered higher $^{87}Sr/^{86}Sr$ values after 5 Ma could reflect both greater degrees of erosion from accreted continental units, but also higher degrees of chemical weathering (Derry & France-Lanord 1996), as implied by the Mg/Al, K/Al, and CIA records.

The noisy character of the Nd isotope record since 5 Ma may indicates rapid changes in the patterns of erosion or even changes in drainage organization and/or the location of delivery of the sediment into the Gulf of Papua. Either way, the general trend is towards a decrease in the relative erosional flux from the arc-ophiolite crust. The Sr isotopes are broadly consistent with this interpretation. The moderate decrease in $^{87}Sr/^{86}Sr$ values between

23 and 8 Ma is what might be expected from increasing erosion from primitive arc or ophiolite crust. Likewise, the increase in $^{87}Sr/^{86}Sr$ values to higher values after 7 Ma could reflect both greater degrees of erosion from accreted continental units, as well as higher degrees of chemical weathering.

The fact that the earliest orogenic sediments at Site 210 are arc-ophiolite derived mirrors the igneous-sourced sediments of the Fanshuliao Formation at the start of the Taiwan collision, where there was a similar progression to more erosion of the deformed passive margin as collision continued (Paliwan Formation)(Dorsey 1988; Teng *et al.* 1988). Isotope evidence in this study requires more recycling of accreted Australia crust starting ~7 Ma, accompanied by increasing Ti and Zr contents, getting much stronger after 5 Ma and peaking at the present day. This flux comes from the accreted Australian rocks in the Fold and Thrust Belt, as well as the Pliocene-Recent exposure of metamorphic rocks in the Owen Stanley Range. It is interesting to note that the amount of continental crustal recycling is much lower in New Guinea than it is in Taiwan. Rivers draining modern Taiwan have $\varepsilon_{Nd}$ values of around -9 to -14 (Lan *et al.* 2002), whereas the lowest value measured at Site 210 is -3.3 (Table 2). This large discrepancy points to much more erosion from arc-ophiolite sources and potentially much more offscraping of these units in New Guinea compared to Taiwan.

*Isotope Mixing*

The isotopic composition of the sediments can be used to better constrain the provenance evolution if compared with the isotopic composition of potential bedrock units. Source region isotopic compositions are determined from bedrock analyses compiled from the GEOROC database (Table S5). We use whole rock compositions compiled from the GEOROC database to represent potential source regions. A significant proportion of existing analyses are related to igneous rocks that have been emplaced into the orogenic belt, likely following the delamination of the lower crust and mantle from the subducting Australian slab (Cloos *et al.* 2005). This means that although the GEOROC analyses may be from rocks exposed within Australian or arc-type tectonic units they represent more recent melting of the mantle below these units and are not necessarily characteristic of the rocks that they intrude or overlie. We use analyses taken from the arc itself to define this end member.

Defining the Australian continental isotopic end member is more problematic. Some analyses from the Fold and Thrust Belt, mostly siltstones, have low $\varepsilon_{Nd}$ values and high $^{87}Sr/^{86}Sr$ values, indicative of erosion from older crust. However, these siltstones lie within

the hydrothermal aureole of an igneous intrusion and have been heavily altered by these magmatic activities, so that they may not be representative of the colliding Australian plate (Richards *et al.* 1991). Although they have $\varepsilon_{Nd}$ values that are lower than those of the arc igneous units, they are still rather positive in $\varepsilon_{Nd}$ values for continental crust, especially continental crust associated with Australia (Windrim & McCulloch 1986; Zhao & McCulloch 1995).

Much of northern Australia south of the Torres Strait represents parts of the Northern Australian Craton that would be expected to have much more evolved isotopic compositions (Kumwenda *et al.* 2023). Basement isotopic values from the Mount Isa area located to the southwest of Cape York and which sample the North Australian Craton (McDonald *et al.* 1997) are Archaean but affected by the later 1.8 Ga Barramundi Orogeny (Bierlein *et al.* 2008). However, there is a major boundary within NE Australia between the older Proterozoic rocks to the west and accreted Palaeozoic terranes and orogens to the east. In particular, east of the Proterozoic rocks at Cape York lies the Hodgkinson Province of the Mossman Orogen, a northern equivalent to the Lachlan Orogen of SE Australia (Bultitude *et al.* 1996). This area is characterized by Palaeozoic igneous and metamorphic rocks, together with Neoproterozoic-Early Palaeozoic rocks in the subsurface further south. This major boundary in crustal ages can be extrapolated further north into New Guinea (Davies 2012)(Fig. 1B) so that accreted continental rocks within those regions draining into the Gulf of Papua can be considered to be part of the Palaeozoic. This includes both the sedimentary rocks in the Fold and Thrust Belt, as well as accreted basement blocks and the metamorphic complexes of the Owen Stanley Range.

Although the Hodgkinson Province is deformed in a Palaeozoic Orogen it partly comprises older Neoproterozoic rocks, as well as intrusive Palaeozoic igneous rocks. These new melts represent a mixture between younger mantle melts produced during the orogen and the older crust. As a result, there are two potential end members that might be representative of the Australian crust accreted into the New Guinea mountains on the eastern side of the island. We follow the study of Champion *et al.* (2013), in identifying both an isotopic cluster of Palaeozoic granite as well as an older metasedimentary unit that may be more representative of the crust. The isotopic data available for the Hodgkinson Province is shown in relation to both the arc data compiled from GEOROC, as well as the analysis of the sediments from the Gulf of Papua (Fig. 11).

Sediments from the Gulf of Papua form a mixing line between these evolved "Australian" Hodgkinson Province groups and the arc-ophiolite group. By doing this, we can calculate mixing curves which are also shown on Figure 11 that predict the isotopic composition of a mixture between these end members. In turn we can use these curves to estimate the relative flux from each source to the mixed sediment, taking into account the average concentration of Nd and Sr in the two sources. In general, the sedimentary samples fall closer to the mixing line defined between the arc-ophiolite group and the Hodgkinson Granite end member, which result in higher predicted involvement from Australian crust compared to if we use the metasedimentary end member. To understand the potential uncertainties, we calculate the estimated mixing proportions using both end members (Table 3).

Using the granite end member mixing model we see maximum values of 62% of Australian crust involvement in the sediment at 22.3 Ma, falling to a minimum of 14.7% Australian erosion at 8 Ma and 28% at the present time (Fig. 10D). Using the metasedimentary end member, we have lower predicted involvement from Australian crust, with a maximum of 31% at 22.3 Ma, a minimum of 9% at 8 Ma and a modern-day value of 16.5% (Fig. 10D).

If we consider the outcrop areas in the modern Highlands that drain into the Gulf of Papua, then around 59.5% of the total siliciclastic outcrop (i.e., ignoring the carbonate) comprises Australian rocks and 40.5% of arc-ophiolite rocks. This suggests a lower involvement from arc-ophiolite rocks compared to what is implied from the isotope chemistry, although the discrepancy is less if we consider the granite end member as being more realistic. However, it should be remembered that erosion is not uniform, but typically focused in the highest and steepest parts of any mountain belt, which experience the fastest uplift, resulting in focused preferential erosion. The arc-ophiolite rocks are exposed in the higher parts of the Central Highlands, where the erosion is fastest, so finding that these are more represented in isotope mixing calculations is to be expected.

*Weathering End Members*

The chemical weathering flux into the Gulf of Papua can be quantified if we know both the deposited sediment volumes and the composition of the sediment, as well as the composition of the bedrocks from which it was derived. It is the geochemical difference between the pristine source and the deposited sediment that reflects the degree of alteration that has been achieved, and in turn how much $CO_2$ would be consumed per unit weight of

sediment. As discussed above, the source of the sediment changed through time, being more Australian (continental) in the Early Miocene prior to the collision, then becoming more arc-dominated in the Late Miocene, before a return to a noisy, but often more continental-rich signal since 5 Ma (Fig. 10D). The composition of Australian continental crust can be estimated using an Upper Continental Crust (UCC) average (Rudnick & Gao 2003) in the absence of sufficient suitable bedrock analyses. Much of the basement geochemical data from northeast Australia focuses on relatively young volcanic rocks and is not representative of the bulk crust underthrusting New Guinea. The major element composition of the colliding arc-ophiolites is estimated from analyses from the bedrock in the New Guinea Highlands, together with the ophiolites of the Mobile Belt, and the New Britain Arc (Table S5). These data can be used to provide an average value for the eroding arc-ophiolite crust at any given time using the relative proportions of Australian crust and arc-ophiolite derived from the Sr and Nd isotope data.

By using the compositions of altered sediment relative to fresh source bedrock in terms of the molar ratios of Mg/Al, Ca/Al, Na/Al and K/Al, it is possible to determine how much $CO_2$ is removed per unit weight of weathered rock equivalent (France-Lanord & Derry 1997). The $\Delta CO_2$ values for each isotopically constrained sample are provided in Table 3. The Nd and Sr isotopic data is used to estimate the relative proportion of Arc versus UCC sources for each sample and thus the average major element composition of the bedrock at any given time can be estimated from the end member values. The difference between the bedrock and the sediment Mg/Al, Ca/Al, Na/Al and K/Al values is then used to calculate the $\Delta CO_2$ values using the method of France-Lanord & Derry (1997). If the total volume of sediment was constrained, then the total amount of $CO_2$ consumed could also be calculated for any given time interval. In many samples there is a negative difference in the K/Al values, which should be impossible because this implies that the sediment is fresher than the bedrock source. This discrepancy is caused by reverse weathering where K is fixed into the deposited marine sediment in the form of diagenetic clay minerals, e.g., smectite (Dunlea *et al.* 2017; Mackenzie & Kump 1995). This process is hard to correct for accurately, although this is not a serious source of error because the amount of this negative difference is quite small and because K contributes a relatively moderate amount to the total $CO_2$ consumption. Its contribution is weighted as just 10% compared to the $CO_2$ consumption by Mg and Ca (France-Lanord & Derry 1997). By simply accepting the negative $\Delta$K/Al values we also make a correction for the reverse weathering and the $CO_2$ that is emitted during that process.

It is not possible to make a correction for carbonate weathering which also releases $CO_2$, but there is only a limited amount of carbonate in the Fold and Thrust Belt (~15% of the total; Table 1) so that we conclude that this may be significant but is unlikely to dominate the erosional flux. Burial of organic carbon may also be important in understanding the impact of erosion in this region on atmospheric $CO_2$ consumption. Measurements from the DSDP Site 210 core show that organic carbon contents have risen to ~1.3% since 1 Ma, but that organic carbon contents prior to 2 Ma were less than 0.5% and ~0.1% for the rest of the core (Shipboard Scientific Party 1973). This level suggests that the Gulf of Papua may not be a significant repository of organic carbon prior to the Pleistocene.

Because not all the samples have accompanying isotopic data that can define the relative flux from Australian crust and the arc-ophiolite we assume that those samples deposited between analysed samples had the same sources as the youngest underlying sample. Because large-scale evolution in erosion patterns changes on relatively long timescales in response to tectonically driven rock uplift, it is a reasonable approximation to assume that sediments deposited close in time to the isotopically constrained samples might have the same proportion of source rocks.

Each sediment sample has a unique major element composition, so that each sample also has its own $\Delta CO_2$ value and this can be variable on short timescales. In order to look at long-term variability in chemical weathering we consider a time-averaged value for $\Delta CO_2$ based on the ages of commonly interpreted seismic reflections that can be used in the future to estimate total erosional flux. These dated packages largely correspond to epoch and sub-epoch boundaries. Averaging $\Delta CO_2$ values within such time packages results in values that are applicable over geologically relevant time intervals.

*Comparison with Himalayan Rivers*

We compare our estimates of $\Delta CO_2$ value for weathering New Guinea source rocks with recently calculated estimates for the Indus and Bengal fans, the primary sedimentary depocentres for erosion of the Himalaya (Clift *et al.* 2023)(Fig. 12). We do this because of models that argue that silicate weathering of sediment eroded from the Himalaya could have removed enough $CO_2$ from the atmosphere to have caused much of the Cenozoic global cooling (Raymo & Ruddiman 1992). Others have argued for the islands of SE Asia as being more important because of their great size (New Guinea is approximately the same length as the Himalayas), their reactive mafic composition, and the significant sediment production

(Bayon *et al.* 2023). The Fly River is smaller than the Asian drainages but if we sum the three largest eastern New Guinea rivers (Fly, Aure and Purari) then the estimated sediment delivery to the ocean in the pre-industrial recent is 245 Mt/y (Milliman & Syvitski 1992), comparable to the Indus River.

The Bengal Fan has bedrock sources that are close to continental crust averages, resulting in $\Delta CO_2$ values of 0.78–0.92 mol/kg compared to 0.99–1.23 mol/kg in the Indus that has more reactive bedrock sources including mafic igneous rocks are exposed in Kohistan and Karakoram, and 0.78 to 0.98 mol/kg in the Mekong (Clift *et al.* 2023). In comparison New Guinea $\Delta CO_2$ values range from as low as 1.50 mol/kg in the lowermost Miocene assuming the granite end member model and 2.8 mol/kg with the metasedimentary end member. Maximum $\Delta CO_2$ values are estimated for the Pleistocene and are 3.40 and 3.82 mol/kg respectively since 1.8 Ma. These high values reflecting the dominant, mafic source rock compositions and imply that New Guinea weathering has been removing three to four times more $CO_2$ from the atmosphere per unit weight of sediment than erosion in mainland Asia. Determining whether this is a globally significant amount of $CO_2$ for the atmosphere requires an erosion budget, although volumes estimated from the Central Highlands does indicate a globally important figure. A recent study of exhumation in that area suggests that if the cooling recorded in the bedrock sources is largely driven by erosion, then this may have caused ~0.6–1.2 °C of cooling during the Late Miocene (Martin *et al.* 2023).

The K/Si versus Al/Si plot from Lupker *et al.* (2013) accounts for differences in alteration linked to grain size rather than because of environmental controls. Arrays of sediment from any single drainage can be plotted together and the overall slope used to assess average weathering intensity. Data from the Indus (Zhou *et al.* 2021), Mekong (Liu *et al.* 2017) and Bengal (Crowley *et al.* 1998; France-Lanord *et al.* 2016; Tachambalath *et al.* 2023) are used to show how these systems compare. The steep slope for the Bengal Fan data implies that this is the least weathered overall, with the Mekong being similar and the Indus more weathered. The New Guinea sediments are not so well defined because of the limited grain size variability but they show the shallowest gradient, implying that they are the most altered of any of these catchments.

This work indicates high $CO_2$ consumption during silicate weathering in New Guinea and is consistent with recent models that propose increasing reactivity of the Earth surface during the Neogene, as a driver of global cooling (Caves Rugenstein *et al.* 2019). Our results support models that propose uplift and weathering of mafic arc and ophiolite rocks in the

tropics being critical to the control of global climate over geological timescales (Macdonald *et al.* 2019).

*Chemical Weathering Efficiency*

The 245 Mt/y discharge from the larger eastern New Guinea rivers is the minimum amount recently reaching the Gulf of Papua because it does not account for sediment discharge from the smaller rivers in the Papuan Peninsula. Applying the Late Pleistocene $CO_2$ consumption rate to this 245 Mt/y rate implies 0.72 Tmol/y of $CO_2$ drawdown or ~8.6 Mt of carbon per year. Considering just the Fly River with an average load of 115 Mt/y of sediment, the weathering driven $CO_2$ consumption would average 0.34 Tmol/y or 4.0 Mt/y. In comparison, recent estimates that integrate the Indus, Bengal, Mekong, and Pearl river systems in south and Southeast Asia result in a collective contribution to the global carbon budget of 0.72–1.07 Tmol/y (Clift *et al.* 2023). This modern rate of $CO_2$ consumption in New Guinea would represent ~7% of the global average Holocene consumption (3.3% if we just consider the Fly River). The total $CO_2$ consumption rate would be higher again if we were able to account for the fluxes in the smaller rivers of the Papuan Peninsula. Weathering studies of small rivers draining mafic and ultramafic sources in the Philippines emphasize that these can be very significant to regional carbon budgets (Schopka *et al.* 2011).

Our values can be compared with measurements from modern river water. Gaillardet *et al.* (1999) estimate only 0.049 Tmol/y of silicate related weathering in the modern Fly River, with an additional 0.066 Tmol/y linked to carbonate, much less than estimated here. This discrepancy could indicate that the river changes weathering flux through time, potentially linked to climate change. Depending on when the water samples were taken, it is possible that the river water is not even representative of the modern weathering state when the climate is seasonal. Carbonate and pyrite weathering could offset the estimated silicate-related flux but are part of a different cycle linked more strongly to organic burial and oxygen and are not considered here. Alternatively, we suggest that some of the net weathering recorded offshore may occur downstream of where the modern river waters were sampled. Weathering is expected to be strongest on flood plains and on exposed continental shelves during glacially induced sea level low stands. Some of the alteration may occur on the seafloor after deposition and before burial. If so then weathering flux estimates based on modern river water may not be applicable over long time spans.

## Conclusions

Sediments deposited in the Gulf of Papua and sampled at DSDP Sites 210 and 287 record the history of erosion and weathering of eastern New Guinea dating back to ~25 Ma. Nd and Sr isotope data show that erosion from Australia was strong at the base of the clastic section during the Early Miocene, likely sourced directly from the Australia passive margin. High Ni values in the Early Miocene may reflect erosion of tropical laterites developed on the exposed ultramafic units of the colliding arc. The Sr and Nd data show increasing erosion from arc and ophiolite rocks into the Middle Miocene driven by erosion of uplifting arc units during the collision between Australia and the North Coast Range-New Britain Arc starting after ~15 Ma. Erosion from arc-ophiolite rocks reached a peak in the Middle-Late Miocene and then began to reduce as a proportion of the total flux after ~7 Ma. Instead, increased erosion from offscraped and unroofed Australian plate continental rocks drove higher Zr and Ti contents after ~7 Ma. The proportion of erosion from Australian plate continental rocks increased during the Pliocene and Pleistocene but was quite variable. The overall trend is like that seen in the Taiwan arc-continent collision but with much more erosion from the arc-ophiolite in New Guinea.

A variety of element chemical weathering indices and proxies show a relatively stable degree of chemical alteration of sediment deposited prior to ~5 Ma followed by an increase to the present day. At the same time kaolinite increased in its proportion of the total clay assemblage, especially after 5 Ma, while smectite shows a mirror image decreasing trend. The stronger chemical weathering is inferred to take place under progressively more tropical conditions, while there is no clear trend to relatively more or less physical erosion versus chemical weathering. The trend to more alteration is at odds with the opposite trend seen in many mainland Asian delta-fan systems.

Current lack of a volumetric budget for the sediment reaching the Gulf of Papua over geological timescales means that it is not possible to calculate the evolving chemical weathering of flux related to the breakdown of silicate minerals. However, it is possible to demonstrate that chemical weathering in New Guinea was more intense than that seen in the Indus, Bengal, or Mekong basins on average. Using the radiogenic isotope data to estimate the relative proportion of erosion from Australian crust versus arc rocks and the average major element compositions for both these end members allows the amount of $CO_2$ that would be consumed per unit volume of sediment deposited to be estimated. This value was substantially higher in New Guinea than seen in mainland Asia, consistent with the idea that

weathering of the mafic igneous islands of Southeast Asia is an important process in the reduction of atmosphere $CO_2$ and in turn global cooling.

Using modern discharge data implies that the Pleistocene weathering flux is similar in magnitude to that calculated for the Ganges-Brahmaputra and that it has been increasing since the start of the Pliocene. This estimate does not however consider the release of $CO_2$ caused by weathering of pyrite-bearing and carbonate rocks, or the oxidation of rock organic carbon. This may partly account for the mismatch between the weathering flux estimated in this study and that derived from the measurement of modern water chemistry in the rivers. Alternatively, it is possible, the chemical weathering is relatively weak at the present time compared to the Pleistocene average, or that a lot of the chemical weathering takes place further downstream from where the river was sampled. Reconciling the modern and ancient data is important for calculating long-term carbon budgets for this and other drainage basins, which is necessary if we are to understand their role in controlling global climate over tectonic timescales.

**Acknowledgements**

PC thanks the Hanse Wissenschaftskolleg for providing the opportunity to work on these topics. We thank International Ocean Discovery Program for providing the samples used in this work. The Charles T. McCord Chair in Petroleum Geology at LSU supported some of the analytical and travel costs. We thank Amy Gough and an anonymous reviewer for their help in improving the initial submission.

**Figure Captions**

**Figure 1.** Bathymetric, topographic and geologic maps of eastern New Guinea and surrounding regions. A) Shaded map showing geographic features together with the location of the sites used in this study. Bathymetric contours are shown at 1000 m intervals. Base map generated by *GeoMapApp.* B) Simplified geological map of New Guinea overlain by the major modern rivers supplying sediment to the Gulf of Papua. Units of the Palaeozoic Basement, Fold and Thrust Belt, Aure Accretionary Prism and metamorphic rocks of the Papuan Peninsula are affiliated with the Australian continental block. Modified from Davies (2012) and Baldwin et al. (2012).

**Figure 2.** Stratigraphic columns of the drilled sections. Stratigraphic columns of the drilled sections at DSDP Sites 210 (Shipboard Scientific Party 1973) and 287 (Shipboard Scientific Party 1975), showing the average sediment types and age assignments from the shipboard reports, as well as carbonate for Site 210 and mean grain size from this work.

**Figure 3.** Temporal evolution in A) mean grain size and B) kurtosis of sediment samples analyzed from DSDP Sites 210 and 287.

**Figure 4.** A) Cross plot of the Chemical Index of Alteration (Nesbitt *et al.* 1980) versus mean green size, showing the pool correlation between green size and chemical alteration in the considered samples. B) and cross-plot against Mg/Al which is a more effective, proxy of weathering in mafic rocks, that dominate the Highlands in the catchments draining into the Gulf of Papua.

**Figure 5**. A) Geochemical signature of the analyzed samples illustrated by a CN-A-K ternary diagram (Fedo *et al.* 1995). Samples closer to $Al_2O_3$ are rich in kaolinite, chlorite and/or gibbsite (representing by Kao, Chl and Gib). CIA values are also calculated and shown on the left side. Abbreviations: sm (smectite), pl (plagioclase), ksp (K-feldspar), il (illite), m (muscovite). B) Geochemical characterization of the sediments analysed in this study following the scheme of Herron (1988).

**Figure 6.** Temporal evolution in chemical weathering proxies. A) Index of Compositional Variability (Cox *et al.* 1995), B) CIX from Garzanti *et al.* (2014), C) CIA from Nesbitt *et al.*

(1980), D) K/Al, E) K/Rb, F) Na/Al, G) Mg/Al and H) Ca/Al. Darker symbols show data from DSDP Site 210 and lighter symbols from DSDP Site 287.

**Figure 7.** Temporal evolution in chemical weathering proxies normalized to sedimentation rates. A) CIA from Nesbitt *et al.* (1980), B) CIX from Garzanti *et al.* (2014), C) Mg/Al and D) L/Al. Darker symbols show data from DSDP Site 210 and lighter symbols from DSDP Site 287.

**Figure 8.** Geochemical proxies linked to sediment provenance. A) Zr as a proxy for zircon content, B) Ti as a proxy for rutile and ilmenite contents, C) Cr as a proxy for spinel content, D) Ni as a proxy for ultramafic rocks and laterites, E) $^{87}Sr/^{86}Sr$ and F) $\varepsilon_{Nd}$ values.

**Figure 9.** Temporal evolution in the abundance of environmentally sensitive clay minerals. A) kaolinite, associated with tropical weathering, B) smectite, associated with the weathering of volcanic rocks and in seasonal climate, C) smectite/(illite + chlorite), a proxy for the relative strength of chemical weathering versus physically erosion, and D) smectite/kaolinite, a proxy for the relative strength of seasonal versus tropical weathering.

**Figure 10.** Temporal evolution in A) weathering intensity tracked by Mg/Al, and B) kaolinite content. Provenance proxies C) Zr content, and D) proportion of Australian erosion in the sediment estimated from Sr and Nd isotopes (light blue from Palaeozoic granite end member and dark blue from Palaeozoic metamorphic rock end member (see Fig. 10). E) Benthic foraminifer oxygen isotope values from Westerhold *et al.* (2020) as a proxy for ocean temperature.

**Figure 11.** Isotopic constraints on sediment source. Cross plot of Nd and Sr isotope compositions for samples from DSDP Site 210 together with bedrock analyses from the GEOROC database. Two isotopic mixing lines are shown between plausible end members with italic numbers showing the percentage of arc crust contributing relative to recycled Australian crust.

**Figure 12.** Estimated development in bedrock reactivity. Temporal evolution in the reactivity of silicate sources within the large drainage systems of the Indian Ocean (Clift *et al.* 2023)

compared to that from the Gulf of Papua. The two lines for New Guinea (NG) show the range possible values depending on whether the continental sources are dominated by Hodgkinson Province granites or metasedimentary rocks.

**Figure 13.** Cross plot of K/Si versus Al/Si from Lupker *et al.* (2013). Al/Si is a proxy for grain size so that average alteration intensity can be estimated from the slope of the array. Indus data from Zhou *et al.* (2021), Mekong data from Liu *et al.* (2017) and Bengal data from Tachambalath *et al.* (2023), Crowley *et al.* (1998) and France-Lanord *et al.* (2015)

**Table 1.** Total map area of the various tectonic units mapped by Davies (2012), showing the proportion of the different units whose drainage flows into the Gulf of Papua.

**Table 2.** Isotope data. Sr and Nd isotopic analyses of samples used in this study.

**Table 3.** Calculated values of Australian crustal contribution to the mixed sediment based on two possible end members for the geology of NE Australian Palaeozoic crust, and the associated time averaged $\Delta CO_2$.

**Table 4**. Major element composition of the end member bedrock sources used to calculate weathering rate.

## References


Abbott, L.D., Silver, E.A. & Galewsky, J. 1994a. Structural evolution of a modern arc-continent collision in Papua New Guinea. *Tectonics*, **13**, 1007–1034.

Abbott, L.D., Silver, E.A., Thompson, P.R., Filewicz, M.V., Schneider, C. & Abdoerrias. 1994b. Stratigraphic constraints on the development and timing of arc-continent collision in northern Papua New Guinea. *Journal of Sedimentary Research*, **64**, 2b, 169-183, doi:10.1306/d4267f82-2b26-11d7-8648000102c1865d.

Alizai, A., Hillier, S., Clift, P.D. & Giosan, L. 2012. Clay mineral variations in Holocene terrestrial sediments from the Indus Basin; a response to SW Asian Monsoon variability. *Quaternary Research*, **77**, 3, 368–381, doi:10.1016/j.yqres.2012.01.008.

Anthony, J.W., Bideaux, R.A., Bladh, K.W. & Nichols, M.C. 2022. Ilmenite. *Handbook of Mineralogy*. Mineralogical Society of America, Chantilly, VA, USA.

Baldwin, S.L., Fitzgerald, P.G. & Webb, L.E. 2012. Tectonics of the New Guinea Region. *Annual Review of Earth and Planetary Sciences*, **40**, 495–520.

Bayon, G., Patriat, M., Godderis, Y., Trinquier, A., De Deckker, P., Kulhanek, D.K., Holbourn, A. & Rosenthal, Y. 2023. Accelerated mafic weathering in Southeast Asia linked to late Neogene cooling. *Science Advances*, **9**, 13, eadf3141, doi:10.1126/sciadv.adf3141.

Berner, R.A. & Berner, E.K. 1997. Silicate weathering and climate. *In*: Ruddiman, W.F. (ed.) *Tectonic Uplift and Climate Change*. Springer, New York, 353–365.

Bierlein, F.P., Black, L.P., Hergt, J. & Mark, G. 2008. Evolution of Pre-1.8Ga basement rocks in the western Mt Isa Inlier, northeastern Australia—Insights from SHRIMP U–Pb dating and in-situ Lu–Hf analysis of zircons. *Precambrian Research*, **163**, 1, 159-173, doi:10.1016/j.precamres.2007.08.017.

Biscaye, P.E. 1965. Mineralogy and sedimentation of recent deep-sea clay in the Atlantic Ocean and adjacent seas and oceans. *Geological Society of America Bulletin*, **76**, 803–832.

Bouchez, J., Gaillardet, J., Lupker, M., Louvat, P., France-Lanord, C., Maurice, L., Armijos, E. & Moquet, J.-S. 2012. Floodplains of large rivers: Weathering reactors or simple silos? *Chemical Geology*, **332-333**, 166-184.

Brown, C.M., Pigram, C.J. & Skwarko, S.K. 1979. Mesozoic stratigraphy and geological history of Papua New Guinea. *Palaeogeography, Palaeoclimatology, Palaeoecology*, **29**, 301-322, doi:10.1016/0031-0182(79)90087-7.

Brown, D., Ryan, P.D., Afonso, J.C., Boutelier, D., Burg, J.P., Byrne, T., Calvert, A., Cook, F., DeBari, S., Dewey, J.F., Gerya, T.V., Harris, R., Herrington, R., Konstantinovskaya, E., Reston, T. & Zagorevski, A. 2011. Arc–Continent Collision: The Making of an Orogen. *Arc-Continent Collision*. Springer Berlin Heidelberg, Berlin, Heidelberg, 477-493, doi:10.1007/978-3-540-88558-0_17.

Bufe, A., Hovius, N., Emberson, R., Rugenstein, J.K.C., Galy, A., Hassenruck-Gudipati, H.J. & Chang, J.-M. 2021. Co-variation of silicate, carbonate and sulfide weathering drives CO2 release with erosion. *Nature Geoscience*, **14**, 4, 211-216, doi:10.1038/s41561-021-00714-3.

Bulois, C., Pubellier, M., Chamot-Rooke, N. & Delescluse, M. 2018. Successive Rifting Events in Marginal Basins: The Example of the Coral Sea Region (Papua New Guinea). *Tectonics*, **37**, 1, 3-29, doi:10.1002/2017TC004783.

Bultitude, R.J., Rees, I.D., Garrad, P.D., Champion, D.C. & Fanning, C.M. 1996. *Mossman second edition. Queensland. 1:250 000. Geological Series—Explanatory Notes*.

Byrne, T., Chan, Y.-C., Rau, R.-J., Lu, C.-Y., Lee, Y.-H. & Wang, Y.-J. 2011. The arc-continent collision in Taiwan. *In*: Brown, D. & Ryan, P.D. (eds.) *Arc-continent collision*. Springer-Verlag, Berlin, Frontiers in Earth Sciences, 213–245.

Calmels, D., Gaillardet, J.r.m., Brenot, A.s. & France-Lanord, C. 2007. Sustained sulfide oxidation by physical erosion processes in the Mackenzie River basin: Climatic perspectives. *Geology*, **35**, 11, 1003-1006, doi:10.1130/g24132a.1.

Caves, J.K., Jost, A.B., Lau, K.V. & Maher, K. 2016. Cenozoic carbon cycle imbalances and a variable weathering feedback. *Earth and Planetary Science Letters*, **450**, 152-163, doi:10.1016/j.epsl.2016.06.035.

Caves Rugenstein, J.K., Ibarra, D.E. & von Blanckenburg, F. 2019. Neogene cooling driven by land surface reactivity rather than increased weathering fluxes. *Nature*, **571**, 7763, 99-102, doi:10.1038/s41586-019-1332-y.

Champion, D.C. & Bultitude, R.J. 2013. The geochemical and SrNd isotopic characteristics of Paleozoic fractionated S-types granites of north Queensland: Implications for S-type granite petrogenesis. *Lithos*, **162-163**, 37-56, doi:10.1016/j.lithos.2012.11.022.

Clift, P., D., Jonell, T.N., Du, Y. & Bornholdt, T. 2023. The Impact of Himalayan-Tibetan Erosion on Silicate Weathering and Organic Carbon Burial. *Chemical Geology*, **in review**.

Clift, P.D. & Jonell, T.N. 2021. Himalayan-Tibetan Erosion is not the Cause of Neogene Global Cooling. *Geophysical Research Letters*, **48**, 8, e2020GL087742, doi:10.1029/2020GL087742.

Clift, P.D., Schouten, H. & Vannucchi, P. 2009a. Arc-Continent Collisions, Subduction Mass Recycling and the Maintenance of the Continental Crust. *In*: Cawood, P. & Kroener, A. (eds.) *Accretionary Orogens in Space and Time*. Geological Society, London, **318**, 75–103.

Clift, P.D., Vannucchi, P. & Phipps Morgan, J. 2009b. Crustal redistribution, crust-mantle recycling and Phanerozoic evolution of the continental crust. *Earth Science Reviews*, **97**, 80-104, doi:10.1016/j.earscirev.2009.10.003.

Clift, P.D., Wan, S. & Blusztajn, J. 2014. Reconstructing Chemical Weathering, Physical Erosion and Monsoon Intensity since 25 Ma in the northern South China Sea: A review of competing proxies. *Earth-Science Reviews*, **130**, 86-102, doi:10.1016/j.earscirev.2014.01.002.

Cloos, M., Sapiie, B., van Ufford, A.Q., Weiland, R.J., Warren, P.Q. & McMahon, T.P. 2005. Collisional Delamination in New Guinea: The Geotectonics of Subducting Slab Breakoff. Geological Society of America, , Special Paper, **400**, 1-51.

Cohen, B.E., Knesel, K.M., Vasconcelos, P.M. & Schellart, W.P. 2013. Tracking the Australian plate motion through the Cenozoic: Constraints from 40Ar/39Ar geochronology. *Tectonics*, **32**, 5, 1371-1383, doi:10.1002/tect.20084.

Colin, C., Turpin, L., Bertaux, J., Desprairies, A. & Kissel, C. 1999. Erosional history of the Himalayan and Burman ranges during the last two glacial-interglacial cycles. *Earth and Planetary Science Letters*, **171**, 4, 647-660.

Cox, R., Lowe, D.R. & Cullers, R.L. 1995. The influence of sediment recycling and basement composition on evolution of mudrock chemistry in the southwestern United States. *Geochimica et Cosmochimica Acta*, **59**, 14, 2919-2940, doi:10.1016/0016-7037(95)00185-9.

Craig, M.S. & Warvakai, K. 2009. Structure of an active foreland fold and thrust belt, Papua New Guinea. *Australian Journal of Earth Sciences*, **56**, 5, 719-738, doi:10.1080/08120090903005360.

Crowley, S.F., Stow, D.A.V. & Croudace, I.W. 1998. Mineralogy and geochemistry of Bay of Bengal deep-sea fan sediments, ODP Leg 116: evidence for an Indian subcontinent contribution to distal fan sedimentation. *In*: Cramp, A., MacLeod, C.J., Lee, S.V. & Jones, E.J.W. (eds.) *Geological Evolution of Ocean Basins: Results from the Ocean Drilling Program*. Geological Society, London, **131**, 151-176.

Dalrymple, R.W., Baker, E.K., Harris, P.T., Hughes, M.G., Sidi, F.H., Nummedal, D., Imbert, P., Darman, H. & Posamentier, H.W. 2003. Sedimentology and Stratigraphy of a Tide-Dominated, Foreland-Basin Delta (Fly River, Papua New Guinea). *In*: Sidi, F.H., Nummedal, D., Imbert, P., Darman, H. & Posamentier, H.W. (eds.) *Tropical Deltas of Southeast Asia—Sedimentology, Stratigraphy, and Petroleum Geology*. SEPM Society for Sedimentary Geology, Tulsa, OK, Special Publication, **76**, 147–173, doi:10.2110/pec.03.76.0147.

Davies, H. & Jaques, A. 1984. Emplacement of ophiolite in Papua New Guinea. *In*: Gass, I.G., Lippard, S.J. & Shelton, A.W. (eds.) *Ophiolites and Oceanic Lithosphere*. Geological Society, London, Special Publications, **13**, 341-349, doi:10.1144/GSL.SP.1984.013.01.2.

Davies, H.L. 2012. The geology of New Guinea - the cordilleran margin of the Australian continent. *International Union of Geological Sciences*, **35**, 1, 87-102, doi:10.18814/epiiugs/2012/v35i1/008.

Davies, H.L. & Smith, I.E. 1971. Geology of Eastern Papua. *GSA Bulletin*, **82**, 12, 3299-3312, doi:10.1130/0016-7606(1971)82[3299:Goep]2.0.Co;2.

Dawson, J.B. & Smith, J.V. 1975. 26 - Chromite-silicate intergrowths in upper mantle peridotites. *In*: Ahrens, L.H., Dawson, J.B., Duncan, A.R. & Erlank, A.J. (eds.) *Physics and Chemistry of the Earth*. Pergamon, 339-350, doi:10.1016/B978-0-08-018017-5.50030-4.

DePaolo, D.J. & Wasserburg, G.J. 1976. Nd isotopic variations and petrogenetic models. *Geophysical Research Letters*, **3**, 5, 249-252.

Derry, L.A. & France-Lanord, C. 1996. Neogene Himalayan weathering history and river $^{87}Sr/^{86}Sr$; impact on the marine Sr record. *Earth and Planetary Science Letters*, **142**, 59-74.

Dessert, C., Dupré, B., Gaillardet, J., Francois, L.M. & Allegre, C. 2003. Basalt weathering laws and the impact of basalt weathering on the global carbon cycle. *Chemical Geology*, **202**, 257–273.

Dewey, J.F. & Bird, J.M. 1970. Mountain belts and the new global tectonics. *Journal of Geophysical Research (1896-1977)*, **75**, 14, 2625-2647, doi:10.1029/JB075i014p02625.

Dorsey, R.J. 1988. Provenance evolution and unroofing history of a modern arc-continent collision; evidence from petrography of Plio-Pleistocene sandstones, eastern Taiwan. *Journal of Sedimentary Research*, **58**, 2, 208-218, doi:10.1306/212f8d5a-2b24-11d7-8648000102c1865d.

Dow, D., Smit, J. & Page, R. 1974. *Wau, Papua New Guinea-1: 250 000 Geological Series.* Bureau of Mineral Resources Australia.

Draut, A.E. & Clift, P.D. 2013. Differential preservation in the geologic record of intraoceanic arc sedimentary and tectonic processes. *Earth Science Reviews*, **116**, 57–84, 10.1016/j.earscirev.2012.11.003.

Dunlea, A.G., Murray, R.W., Santiago Ramos, D.P. & Higgins, J.A. 2017. Cenozoic global cooling and increased seawater Mg/Ca via reduced reverse weathering. *Nature Communications*, **8**, 1, 844, doi:10.1038/s41467-017-00853-5.

Fedo, C.M., Nesbitt, H.W. & Young, G.M. 1995. Unraveling the effects of potassium metasomatism in sedimentary rocks and paleosols, with implications for paleoweathering conditions and provenance. *Geology*, **23**, 921–924.

France-Lanord, C. & Derry, L.A. 1997. Organic carbon burial forcing of the carbon cycle from Himalayan erosion. *Nature*, **390**, 65–67.

France-Lanord, C., Spiess, V., Klaus, A. & Expedition 354 Scientists. 2015. Bengal Fan: Neogene and late Paleogene record of Himalayan orogeny and climate: a transect

across the Middle Bengal Fan. *International Ocean Discovery Program Preliminary Report*, **354**, doi:10.14379/iodp.pr.354.2015.
France-Lanord, C., Spiess, V., Klaus, A., Schwenk, T. & Expedition 354 Scientists. 2016. *Bengal Fan.* International Ocean Discovery Program.
Gaillardet, J., Dupré, B. & Allègre, C.J. 1999. Geochemistry of large river suspended sediments: silicate weathering or recycling tracer? *Geochimica et Cosmochimica Acta*, **63**, 23-24, 4037-4051.
Garçon, M., Chauvel, C., France-Lanord, C., Limonta, M. & Garzanti, E. 2014. Which minerals control the Nd–Hf–Sr–Pb isotopic compositions of river sediments? *Chemical Geology*, **364**, 42-55, doi:10.1016/j.chemgeo.2013.11.018.
Garzanti, E., Vermeesch, P., Padoan, M., Resentini, A., Vezzoli, G. & Andò, S. 2014. Provenance of Passive-Margin Sand (Southern Africa). *The Journal of Geology*, **122**, 1, 17-42, doi:10.1086/674803.
Gleeson, S.A., Butt, C.R.M. & Elias, M. 2003. Nickel Laterites: A Review. *SEG Discovery*, 54, 1-18, doi:10.5382/SEGnews.2003-54.fea.
Golightly, J.P. 1981. Nickeliferous Laterite Deposits. *In*: Skinner, B.J. (ed.) *Seventy-Fifth Anniversary Volume*. Society of Economic Geologists, Littleton, CO, 710-735, doi:10.5382/av75.18.
Gradstein, F.M., Ogg, J.G., Schmitz, M.D. & Ogg, G.M. 2020. Geologic Time Scale 2020. Elsevier Science, pp. 1358.
Hall, R. 2002. Cenozoic geological and plate tectonic evolution of SE Asia and the SW Pacific: computer-based reconstructions and animations. *Journal of Asian Earth Sciences*, **20**, 353-434, doi:10.1016/S1367-9120(01)00069-4.
Harris, R. 2011. The Nature of the Banda Arc–Continent Collision in the Timor Region. *In*: Brown, D. & Ryan, P.D. (eds.) *Arc-Continent Collision*. Springer, Berlin, Heidelberg, 163-211, doi:10.1007/978-3-540-88558-0_7.
Hartmann, J., Jansen, N., Dürr, H.H., Kempe, S. & Köhler, P. 2009. Global CO2-consumption by chemical weathering: What is the contribution of highly active weathering regions? *Global and Planetary Change*, **69**, 4, 185-194, doi:10.1016/j.gloplacha.2009.07.007.
Hartmann, J., Moosdorf, N., Lauerwald, R., Hinderer, M. & West, A.J. 2014. Global chemical weathering and associated P-release — The role of lithology, temperature and soil properties. *Chemical Geology*, **363**, 145-163, doi:10.1016/j.chemgeo.2013.10.025.
Heier, K. & Billings, G. 1970. Rubidium. *In*: Wedepohl, K.H. (ed.) *Handbook of geochemistry*. Springer, Berlin, 37B31–37N31.
Herron, M.M. 1988. Geochemical classification of terrigenous sands and shales from core or log data. *Journal of Sedimentary Petrology*, **58**, 820–829.
Hillier, S. 1995. Erosion, sedimentation, and sedimentary origin of clays. *In*: Velde, B. (ed.) *Clays and the environment*. Springer Verlag, Berlin, 162-219.
Hilton, R.G., Gaillardet, J., Calmels, D. & Birck, J.-L. 2014. Geological respiration of a mountain belt revealed by the trace element rhenium. *Earth and Planetary Science Letters*, **403**, 27-36, doi:10.1016/j.epsl.2014.06.021.
Hilton, R.G., Turowski, J.M., Winnick, M., Dellinger, M., Schleppi, P., Williams, K.H., Lawrence, C.R., Maher, K., West, M. & Hayton, A. 2021. Concentration-Discharge Relationships of Dissolved Rhenium in Alpine Catchments Reveal Its Use as a Tracer of Oxidative Weathering. *Water Resources Research*, **57**, 11, e2021WR029844, doi:10.1029/2021WR029844.
Holbrook, W.S., Lizarralde, D., McGeary, S., Bangs, N. & Diebold, J. 1999. Structure and composition of the Aleutian island arc and implications for continental crustal growth. *Geology*, **27**, 31–34.

Holm, R.J., Spandler, C. & Richards, S.W. 2015. Continental collision, orogenesis and arc magmatism of the Miocene Maramuni arc, Papua New Guinea. *Gondwana Research*, **28**, 3, 1117-1136, doi:10.1016/j.gr.2014.09.011.

Hsieh, H.-H. & Yen, H.-Y. 2016. Three-dimensional density structures of Taiwan and tectonic implications based on the analysis of gravity data. *Journal of Asian Earth Sciences*, **124**, 247-259, doi:10.1016/j.jseaes.2016.05.009.

Hu, D., Clift, P.D., Wan, S., Böning, P., Hannigan, R., Hillier, S. & Blusztajn, J. 2016. Testing chemical weathering proxies in Miocene–Recent fluvial-derived sediments in the South China Sea. *In*: Clift, P.D., Harff, J., Wu, J. & Qiu, Y. (eds.) *River-Dominated Shelf Sediments of East Asian Seas*. Geological Society, London, Special Publication, **429**, doi:10.1144/SP429.5.

Huang, C.Y., Yuan, P.B. & Tsao, S.H. 2006. Temporal and spatial records of active arc-continent collision in Taiwan: A synthesis. *Geological Society of America Bulletin*, **118**, 274–288, doi:doi: 10.1130/B25527.1.

Hülse, P. & Bentley, S.J. 2012. A 210Pb sediment budget and granulometric record of sediment fluxes in a subarctic deltaic system: The Great Whale River, Canada. *Estuarine, Coastal and Shelf Science*, **109**, 41-52, doi:10.1016/j.ecss.2012.05.019.

Jacobsen, S.B. & Wasserburg, G.J. 1980. Sm-Nd isotopic evolution of chondrites. *Earth and Planetary Science Letters* **50**, 1, 139-155.

Jagoutz, O., Macdonald, F.M. & Royden, L. 2016. Low-latitude arc–continent collision as a driver for global cooling. *Proceedings of the National Academy of Sciences*, **113**, 18, 4935–4940, doi: 10.1073/pnas.1523667113.

Jonell, T.N., Li, Y., Blusztajn, J., Giosan, L. & Clift, P.D. 2018. Signal or noise? Isolating grain size effects on Nd and Sr isotope variability in Indus delta sediment provenance. *Chemical Geology*, **485**, 56-73, doi:10.1016/j.chemgeo.2018.03.036.

Kasting, J.F. 2019. The Goldilocks Planet? How Silicate Weathering Maintains Earth "Just Right". *Elements*, **15**, 4, 235-240, doi:10.2138/gselements.15.4.235.

Klootwijk, C., Giddings, J., Pigram, C., Loxton, C., Davies, H., Rogerson, R. & Falvey, D. 2003. North Sepik region of Papua New Guinea: palaeomagnetic constraints on arc accretion and deformation. *Tectonophysics*, **362**, 1, 273-301, doi:10.1016/S0040-1951(02)00641-8.

Kumwenda, J., Betts, P. & Armit, R. 2023. Exposing basement terranes of the North Australian Craton. *Earth-Science Reviews*, **237**, 104310, doi:10.1016/j.earscirev.2022.104310.

Lan, C.Y., Lee, C.-S., Shen, J.J.-S., Lu, C.Y., Mertzman, S.A. & Wu, T.-W. 2002. Nd -Sr isotopic composition and geochemistry of sediments from Taiwan and their implications. *Western Pacific Earth Sciences*, **2**, 2, 205-222.

Li, S.-L., Calmels, D., Han, G., Gaillardet, J. & Liu, C.-Q. 2008. Sulfuric acid as an agent of carbonate weathering constrained by δ13CDIC: Examples from Southwest China. *Earth and Planetary Science Letters*, **270**, 3, 189-199, doi:10.1016/j.epsl.2008.02.039.

Little, T.A., Baldwin, S.L., Fitzgerald, P.G. & Monteleone, B. 2007. Continental rifting and metamorphic core complex formation ahead of the Woodlark spreading ridge, D'Entrecasteaux Islands, Papua New Guinea. *Tectonics*, **26**, 1, doi:10.1029/2005TC001911.

Liu, C., Clift, P.D., Murray, R.W., Blusztajn, J., Ireland, T., Wan, S. & Ding, W. 2017. Geochemical Evidence for Initiation of the Modern Mekong Delta in the southwestern South China Sea after 8 Ma. *Chemical Geology*, **451**, 38–54, doi:10.1016/j.chemgeo.2017.01.008.

Liu, Z., Colin, C., Huang, W., Le, K.P., Tong, S., Chen, Z. & Trentesaux, A. 2007. Climatic and tectonic controls on weathering in south China and Indochina Peninsula: Clay

mineralogical and geochemical investigations from the Pearl, Red, and Mekong drainage basins. *Geochemistry Geophysics Geosystems*, **8, Q05005**, doi:10.1029/2006GC001490.

Lorand, J.P. & Ceuleneer, G. 1989. Silicate and base-metal sulfide inclusions in chromites from the Maqsad area (Oman ophiolite, Gulf of Oman): A model for entrapment. *Lithos*, **22**, 3, 173-190, doi:10.1016/0024-4937(89)90054-6.

Lupker, M., France-Lanord, C., Galy, V., Lave, J., Gaillardet, J., Gajured, A.P., Guilmette, C., Rahman, M., Singh, S.K. & Sinha, R. 2012. Predominant floodplain over mountain weathering of Himalayan sediments (Ganga basin). *Geochimica et Cosmochimica Acta*, **84**, 410-432.

Lupker, M., France-Lanord, C., Galy, V., Lave, J. & Kudrass, H. 2013. Increasing chemical weathering in the Himalayan system since the Last Glacial Maximum. *Earth and Planetary Science Letters*, **365**, 243–252, doi:10.1016/j.epsl.2013.01.038.

Lus, W.Y., McDougall, I. & Davies, H.L. 2004. Age of the metamorphic sole of the Papuan Ultramafic Belt ophiolite, Papua New Guinea. *Tectonophysics*, **392**, 1, 85-101, doi:10.1016/j.tecto.2004.04.009.

Macdonald, F.A., Swanson-Hysell, N.L., Park, Y., Lisiecki, L. & Jagoutz, O. 2019. Arc-continent collisions in the tropics set Earth's climate state. *Science*, **364**, 6436, 181-184, doi:10.1126/science.aav5300.

Mackenzie, F.T. & Kump, L.R. 1995. Reverse Weathering, Clay Mineral Formation, and Oceanic Element Cycles. *Science*, **270**, 5236, 586-586, doi:10.1126/science.270.5236.586.

Maffre, P., Swanson-Hysell, N.L. & Goddéris, Y. 2021. Limited Carbon Cycle Response to Increased Sulfide Weathering Due to Oxygen Feedback. *Geophysical Research Letters*, **48**, 19, e2021GL094589, doi:10.1029/2021GL094589.

Martin, P.E., Macdonald, F.A., McQuarrie, N., Flowers, R.M. & Maffre, P.J.Y. 2023. The rise of New Guinea and the fall of Neogene global temperatures. *Proceedings of the National Academy of Sciences*, **120**, 40, e2306492120, doi:10.1073/pnas.2306492120.

McAlpine, J.R., Keig, G. & Falls, R. 1983. Climate of Papua New Guinea. ANU Press, Canberra, pp. 200.

McDonald, G.D., Collerson, K.D. & Kinny, P.D. 1997. Late Archean and Early Proterozoic crustal evolution of the Mount Isa block, northwest Queensland, Australia. *Geology*, **25**, 12, 1095-1098, doi:10.1130/0091-7613(1997)025<1095:Laaepc>2.3.Co;2.

Metcalfe, I. 2013. Gondwana dispersion and Asian accretion: tectonic and palaeogeographic evolution of eastern Tethys: . *Journal of Asian Earth Sciences*, **66**, 1-33.

Milliman, J.D. & Syvitski, J.P.M. 1992. Geomorphic/tectonic control of sediment discharge to the ocean; the importance of small mountainous rivers. *Journal of Geology*, **100**, 525-544.

Nesbitt, H.W., Markovics, G. & Price, R.C. 1980. Chemical processes affecting alkalis and alkaline earths during continental weathering. *Geochimica et Cosmochimica Acta*, **44**, 1659–1666.

Page, N. 1986. Descriptive model of synorogenic-synvolcanic Ni-Cu. *Mineral deposit models: US Geological Survey Bulletin*, **1693**, 28.

Park, Y., Maffre, P., Goddéris, Y., Macdonald, F.A., Anttila, E.S.C. & Swanson-Hysell, N.L. 2020. Emergence of the Southeast Asian islands as a driver for Neogene cooling. *Proceedings of the National Academy of Sciences*, **117**, 41, 25319-25326, doi:10.1073/pnas.2011033117.

Peng, N., Dang, H., Wu, J., Aiello, I.W. & Jian, Z. 2021. Tectonic and climatic controls on the Plio-Pleistocene evolution of sediment discharge from Papua New Guinea. *Marine Geology*, **441**, 106627, doi:10.1016/j.margeo.2021.106627.

Penman, D.E., Caves Rugenstein, J.K., Ibarra, D.E. & Winnick, M.J. 2020. Silicate weathering as a feedback and forcing in Earth's climate and carbon cycle. *Earth-Science Reviews*, **209**, 103298, doi:10.1016/j.earscirev.2020.103298.

Pigram, C.J., Davies, P.J., Feary, D.A. & Symonds, P.A. 1989. Tectonic controls on carbonate platform evolution in southern Papua New Guinea: Passive margin to foreland basin. *Geology*, **17**, 3, 199-202, doi:10.1130/0091-7613(1989)017<0199:Tcocpe>2.3.Co;2.

Raymo, M.E. & Ruddiman, W.F. 1992. Tectonic forcing of Late Cenozoic climate. *Nature*, **359**, 6391, 117-122, doi:10.1038/359117a0.

Raymo, M.E., Ruddiman, W.F. & Froelich, P.N. 1988. Influence of Late Cenozoic mountain building on ocean geochemical cycles. *Geology*, **16**, 7, 649-653.

Repasch, M., Scheingross, J.S., Hovius, N., Lupker, M., Wittmann, H., Haghipour, N., Gröcke, D.R., Orfeo, O., Eglinton, T.I. & Sachse, D. 2021. Fluvial organic carbon cycling regulated by sediment transit time and mineral protection. *Nature Geoscience*, **14**, 11, 842-848, doi:10.1038/s41561-021-00845-7.

Richards, J.P., McCulloch, M.T., Chappell, B.W. & Kerrich, R. 1991. Sources of metals in the Porgera gold deposit, Papua New Guinea: Evidence from alteration, isotope, and noble metal geochemistry. *Geochimica et Cosmochimica Acta*, **55**, 2, 565-580, doi:10.1016/0016-7037(91)90013-U.

Rosenthal, Y., Holbourn, A.E., Kulhanek, D.K. & Expedition 363 Scientists. 2018. *Western Pacific Warm Pool.* International Ocean Discovery Program.

Rudnick, R.L. 1995. Making continental crust. *Nature*, **378**, 573–578.

Rudnick, R.L. & Gao, S. 2003. The Composition of the Continental Crust. *In*: Rudnick, R.L. (ed.) *The Crust*. Elsevier-Pergamon, Oxford, Treatise on Geochemistry, **3**, 1-64.

Scholl, D.W. & von Huene, R. 2010. Subduction zone recycling processes and the rock record of crustal suture zones. *Canadian Journal of Earth Sciences*, **47**, 633–654, doi:10.1139/E09-061.

Schopka, H.H., Derry, L.A. & Arcilla, C.A. 2011. Chemical weathering, river geochemistry and atmospheric carbon fluxes from volcanic and ultramafic regions on Luzon Island, the Philippines. *Geochimica et Cosmochimica Acta*, **75**, 4, 978-1002, doi:10.1016/j.gca.2010.11.014.

Shipboard Scientific Party. 1973. Site 210. *Initial Reports of the Deep Sea Drilling Project*, **21**, 369-440, doi:10.2973/dsdp.proc.21.110.1973.

Shipboard Scientific Party. 1975. Site 287. *Initial Reports of the Deep Sea Drilling Project*, **30**, 133-173, doi:10.2973/dsdp.proc.30.105.1975.

Smith, I. & Davies, H. 1976. *Geology of the southeast Papuan mainland.* Bureau of Mineral Resources, Geology and Geophysics.

Stein, C.A. & Stein, S. 1992. A model for the global variation in oceanic depth and heat flow with lithospheric age. *Nature*, **359**, 123-129.

Suppe, J. 1984. Kinematics of arc-continent collision, flipping of subduction, and backarc spreading near Taiwan. *In*: Tsan, S.F. (ed.) *A special volume dedicated to Chun-Sun Ho on the occasion of his retirement*, Geological Society of China Memoir, **6**, 21–33.

Tachambalath, A.P., France-Lanord, C., Galy, A., Rigaudier, T. & Charreau, J. 2023. Data report: major and trace element composition of silicates and carbonates from Bengal Fan sediments, IODP Expedition 354. *Proceedings of the International Ocean Discovery Program*, **354**, 1-10, doi:10.14379/iodp.proc.354.204.2023.

Taylor, B., Goodliffe, A.M., Martinez, F. & Hey, R.N. 1995. Continental riting and initial sea-floor spreading in the Woodlark basin. *Nature*, **374**, 534-537.

Tcherepanov, E.N., Droxler, A.W., Lapointe, P., Mohn, K. & Larsen, O.A. 2010. Siliciclastic influx and burial of the Cenozoic carbonate system in the Gulf of Papua. *Marine and Petroleum Geology*, **27**, 2, 533-554, doi:10.1016/j.marpetgeo.2009.09.002.

Teng, L.S., Chen, W.-S., Wang, Y., Song, S.-R. & Lo, H.-J. 1988. Toward a comprehensive stratigraphic system of the Coastal Range, eastern Taiwan. *Acta Geologic Taiwanica*, **26**, 19–35.

Thiry, M. 2000. Palaeoclimatic interpretation of clay minerals in marine deposits; an outlook from the continental origin. *Earth-Science Reviews*, **49**, 1-4, 201-221, doi:10.1016/S0012-8252(99)00054-9.

Tomita, K., Yamane, H. & Kawano, M. 1993. Synthesis of Smectite from Volcanic Glass at Low Temperature. *Clays and Clay Minerals*, **41**, 6, 655-661, doi:10.1346/CCMN.1993.0410603.

Torres, M.A., West, A.J. & Li, G. 2014. Sulphide oxidation and carbonate dissolution as a source of CO2 over geological timescales. *Nature*, **507**, 7492, 346-349, doi:10.1038/nature13030.

van Ufford, A.Q. & Cloos, M. 2005. Cenozoic tectonics of New Guinea. *AAPG Bulletin*, **89**, 1, 119-140, doi: 10.1306/08300403073.

Wan, S., Li, A., Clift, P.D. & Stuut, J.-B.W. 2007. Development of the East Asian monsoon: Mineralogical and sedimentologic records in the northern South China Sea since 20 Ma. *Palaeogeography, Palaeoclimatology, Palaeoecology*, **254**, 3-4, 561–582, doi:10.1016/j.palaeo.2007.07.009.

Webb, M., White, L.T., Jost, B.M. & Tiranda, H. 2019. The Tamrau Block of NW New Guinea records late Miocene–Pliocene collision at the northern tip of the Australian Plate. *Journal of Asian Earth Sciences*, **179**, 238-260, doi:10.1016/j.jseaes.2019.04.020.

Webb, M., White, L.T., Jost, B.M., Tiranda, H. & BouDagher-Fadel, M. 2020. The history of Cenozoic magmatism and collision in NW New Guinea – New insights into the tectonic evolution of the northernmost margin of the Australian Plate. *Gondwana Research*, **82**, 12-38, doi:10.1016/j.gr.2019.12.010.

Weissel, J.K. & Watts, A.B. 1979. Tectonic evolution of the Coral Sea Basin. *Journal of Geophysical Research: Solid Earth*, **84**, B9, 4572-4582, doi:10.1029/JB084iB09p04572.

West, A.J., Galy, A. & Bickle, M.J. 2005. Tectonic and climatic controls on silicate weathering. *Earth and Planetary Science Letters*, **235**, 211–228, doi: 10.1016/j.epsl.2005.03.020.

Westerhold, T., Marwan, N., Drury, A.J., Liebrand, D., Agnini, C., Anagnostou, E., Barnet, J.S.K., Bohaty, S.M., De Vleeschouwer, D., Florindo, F., Frederichs, T., Hodell, D.A., Holbourn, A.E., Kroon, D., Lauretano, V., Littler, K., Lourens, L.J., Lyle, M., Pälike, H., Röhl, U., Tian, J., Wilkens, R.H., Wilson, P.A. & Zachos, J.C. 2020. An astronomically dated record of Earth's climate and its predictability over the last 66 million years. *Science*, **369**, 6509, 1383-1387, doi:10.1126/science.aba6853.

Windrim, D.P. & McCulloch, M.T. 1986. Nd and Sr isotopic systematics of central Australian granulites: chronology of crustal development and constraints on the evolution of lower continental crust. *Contributions to Mineralogy and Petrology*, **94**, 3, 289-303, doi:10.1007/BF00371438.

Wu, F.T., Kuo-Chen, H. & McIntosh, K.D. 2014. Subsurface imaging, TAIGER experiments and tectonic models of Taiwan. *Journal of Asian Earth Sciences*, **90**, 173-208, doi:10.1016/j.jseaes.2014.03.024.

Zack, T. & Kooijman, E. 2017. Petrology and Geochronology of Rutile. *Reviews in Mineralogy and Geochemistry*, **83**, 1, 443-467, doi:10.2138/rmg.2017.83.14.

Zhao, J.-x. & McCulloch, M.T. 1995. Geochemical and Nd isotopic systematics of granites from the Arunta Inlier, central Australia: implications for Proterozoic crustal evolution. *Precambrian Research*, **71**, 1, 265-299, doi:10.1016/0301-9268(94)00065-Y.

Zhou, P., Ireland, T., Murray, R.W. & Clift, P.D. 2021. Marine Sedimentary Records of Chemical Weathering Evolution in the Western Himalaya since 17 Ma. *Geosphere*, **17**, 3, 824–853, doi:10.1130/GES02211.1.

Zondervan, J.R., Hilton, R.G., Dellinger, M., Clubb, F.J., Roylands, T. & Ogrič, M. 2023. Rock organic carbon oxidation CO2 release offsets silicate weathering sink. *Nature*, doi:10.1038/s41586-023-06581-9.

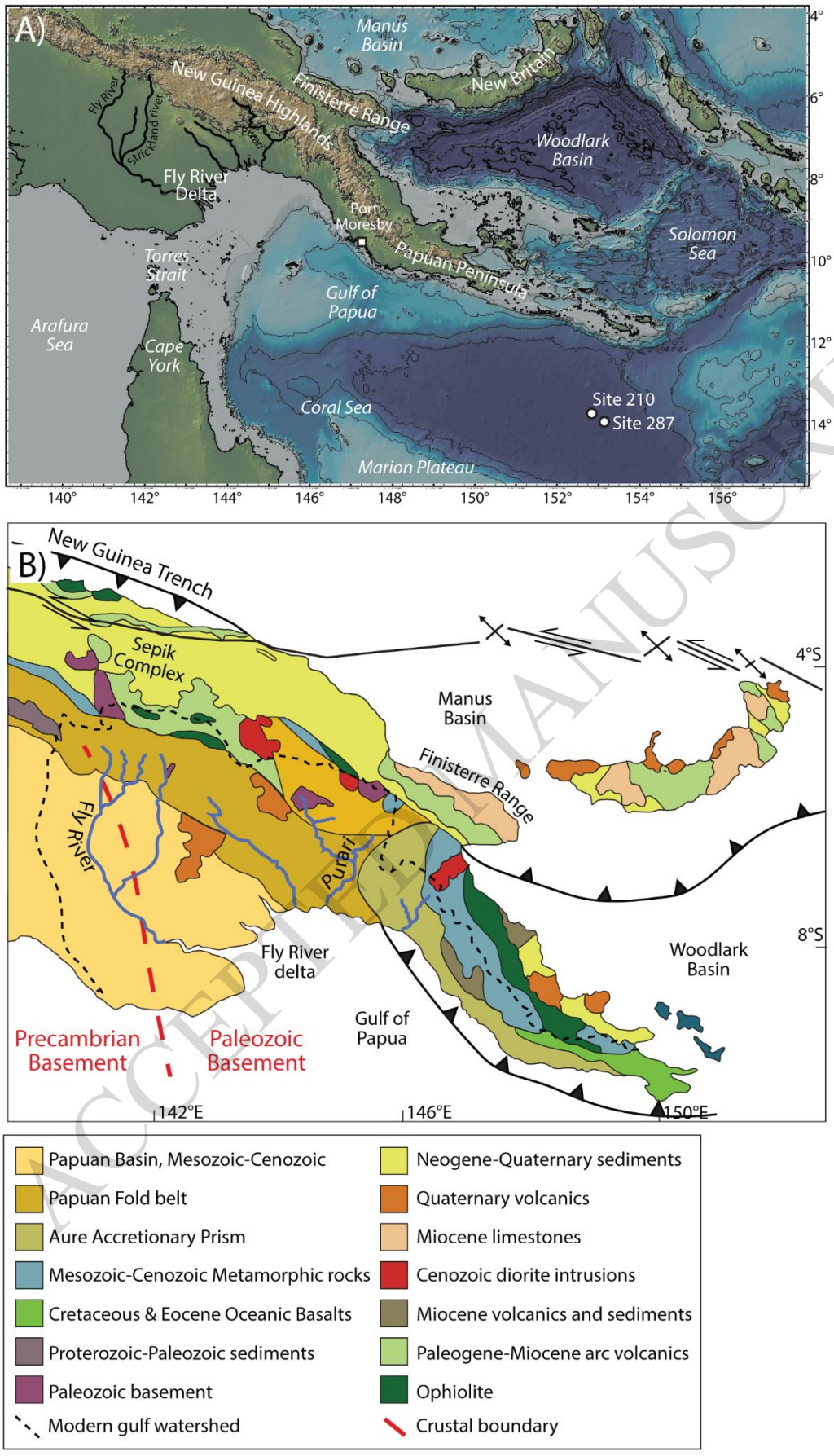


Figure 1

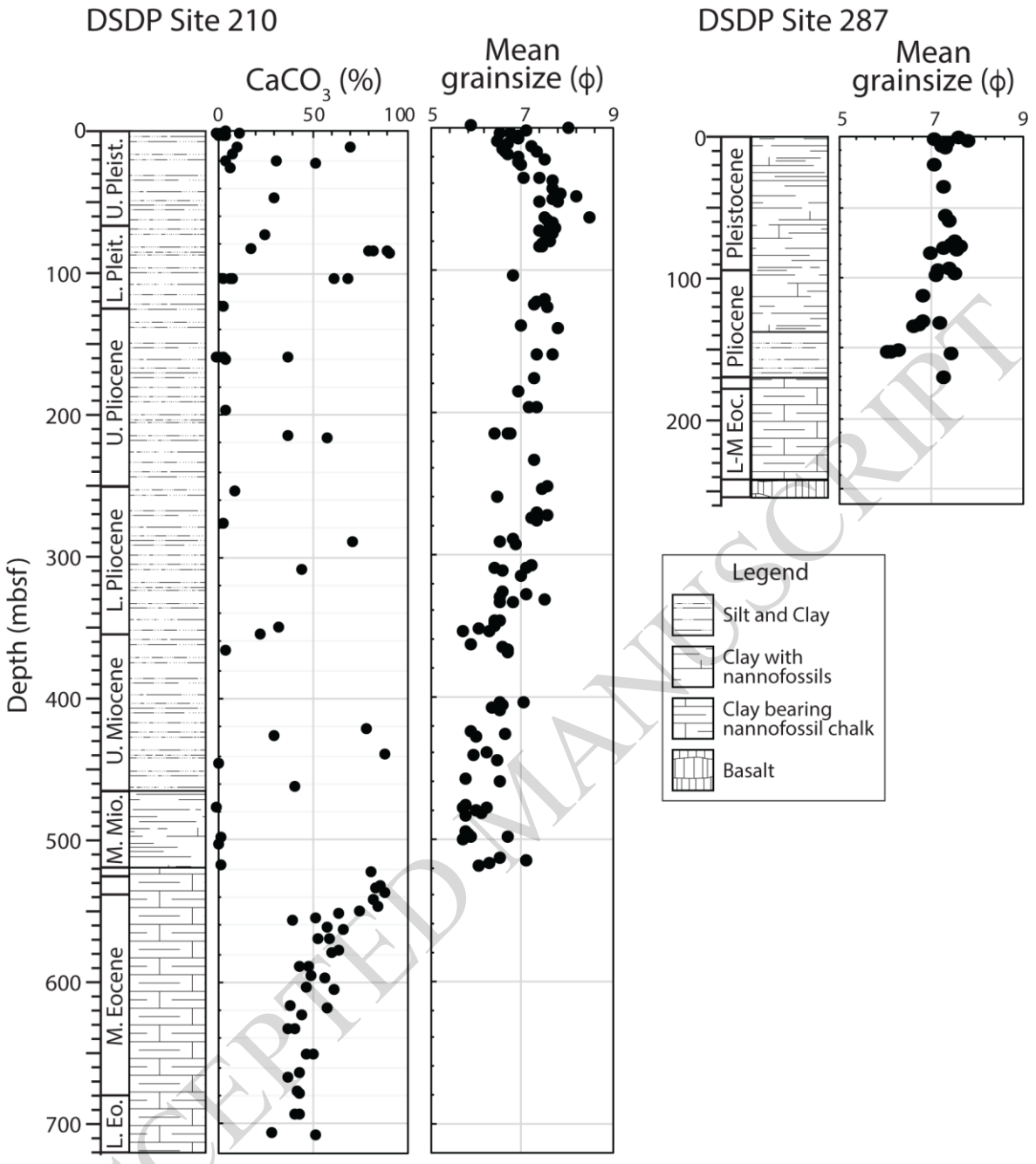


Figure 2

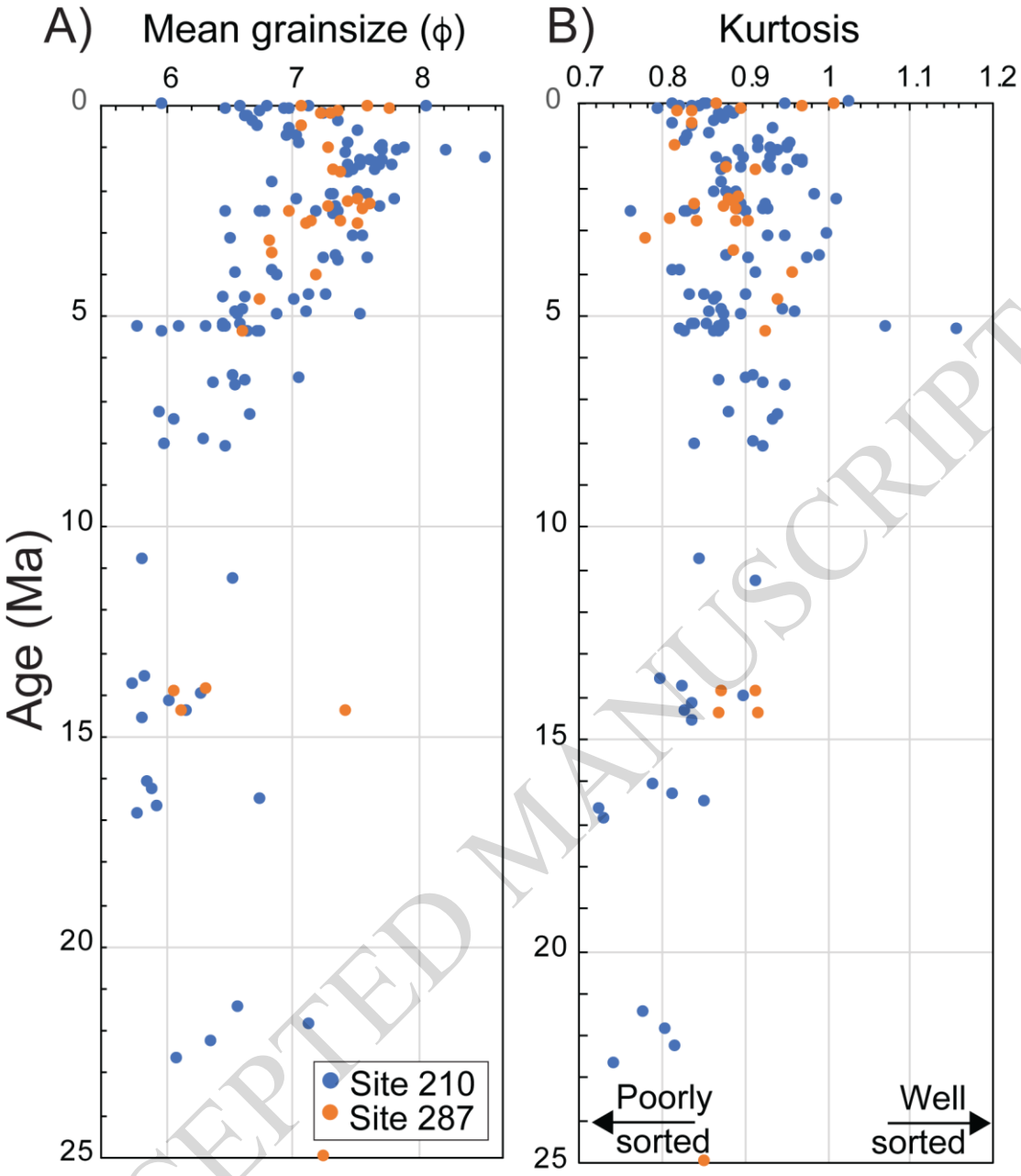


Figure 3

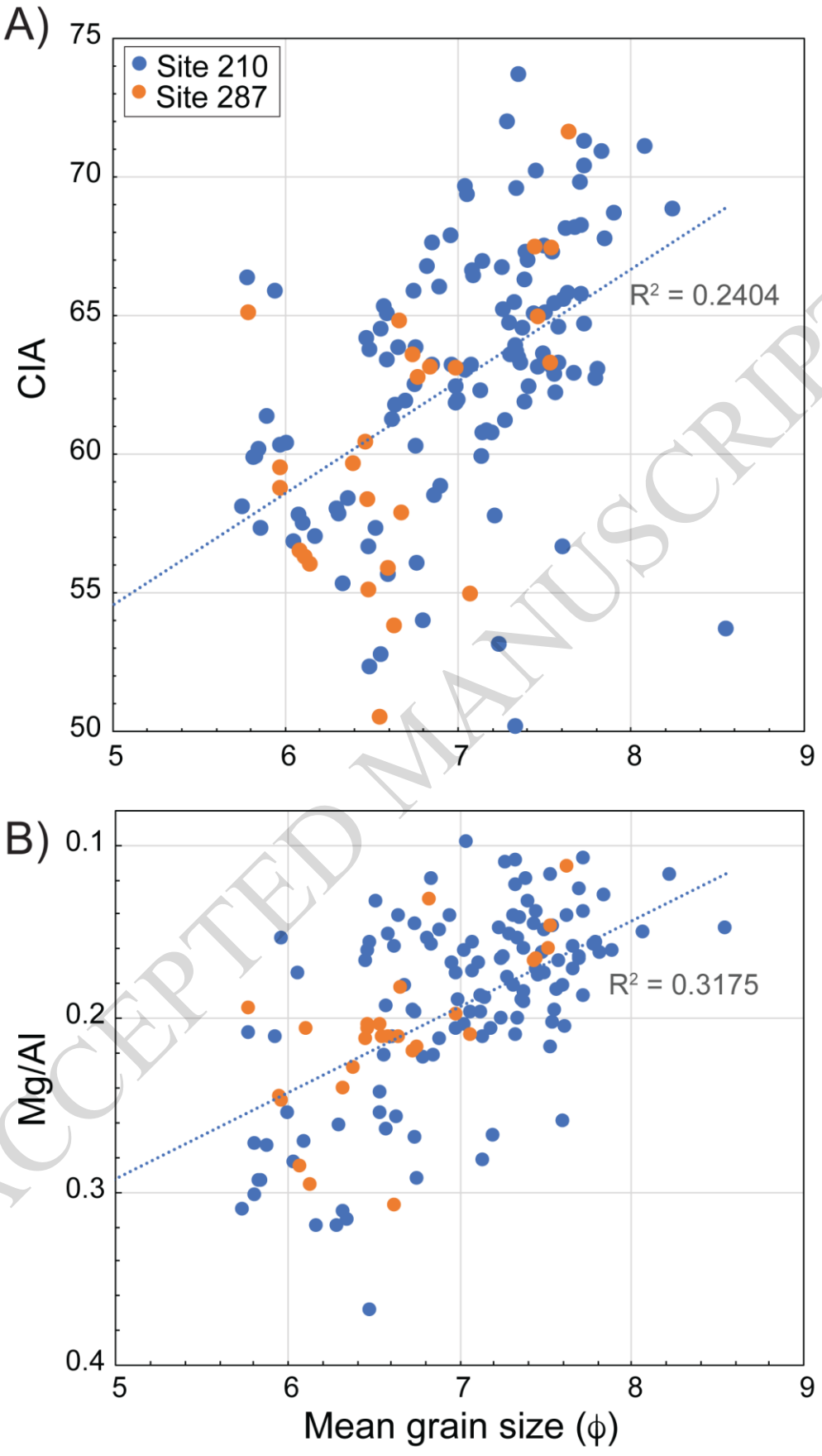


Figure 4

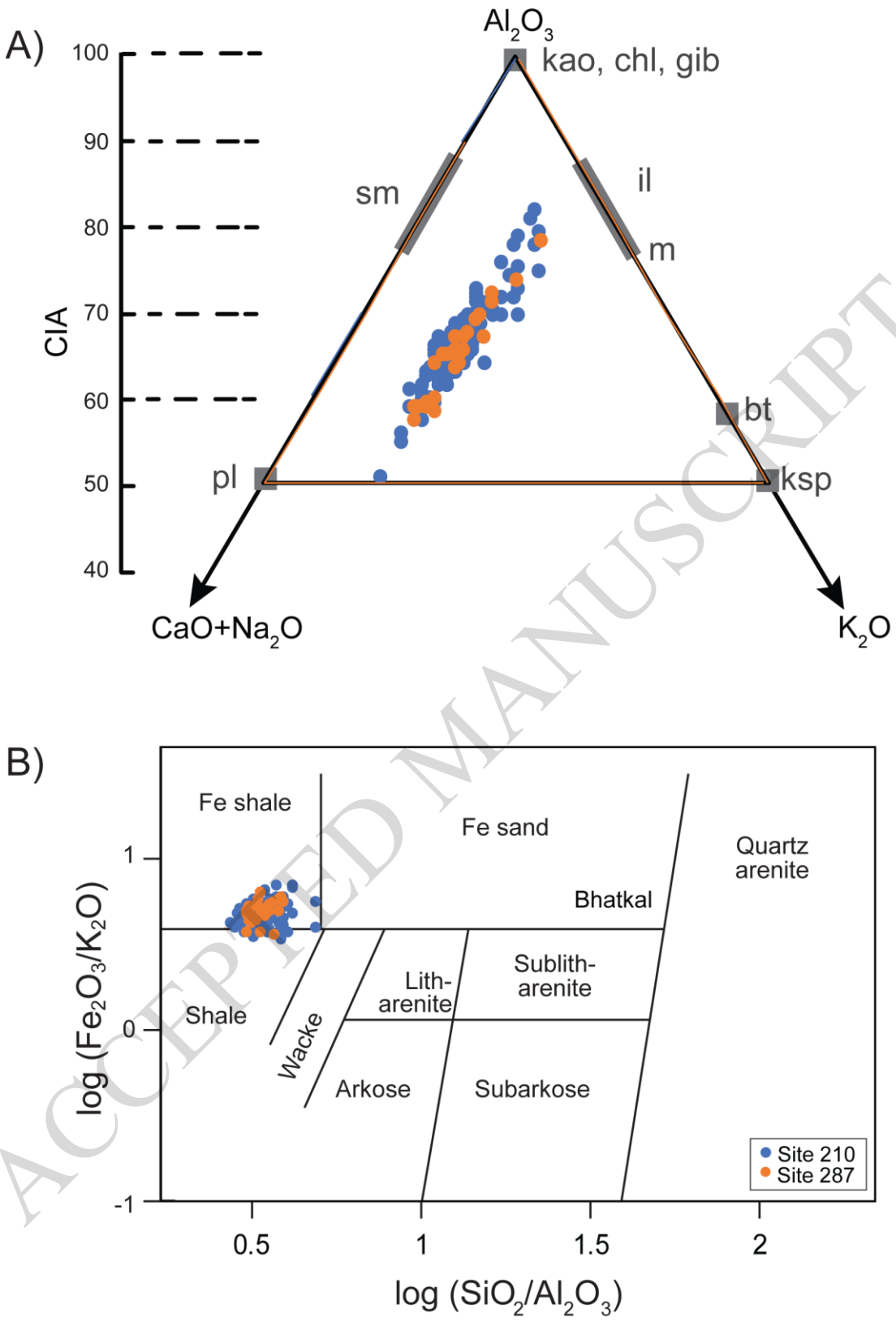


Figure 5

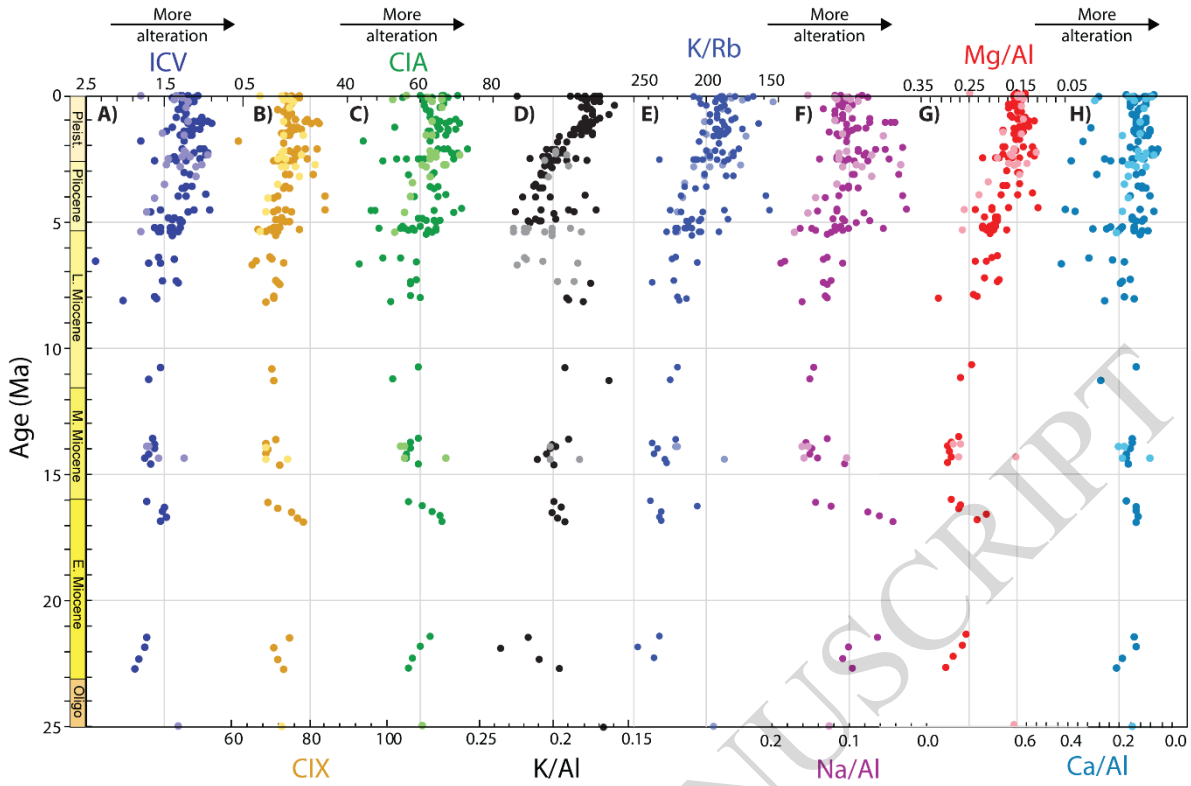


Figure 6

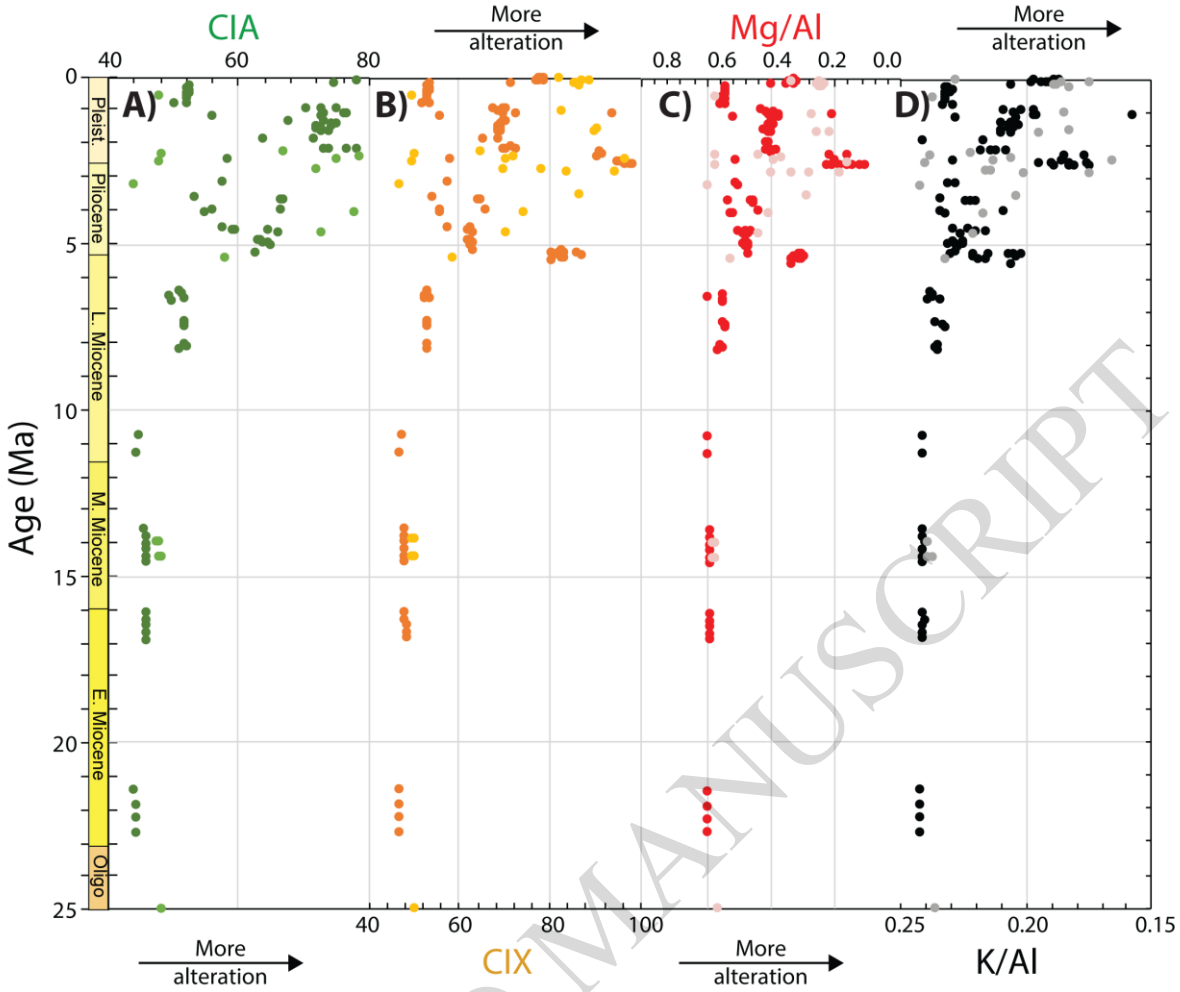


Figure 7

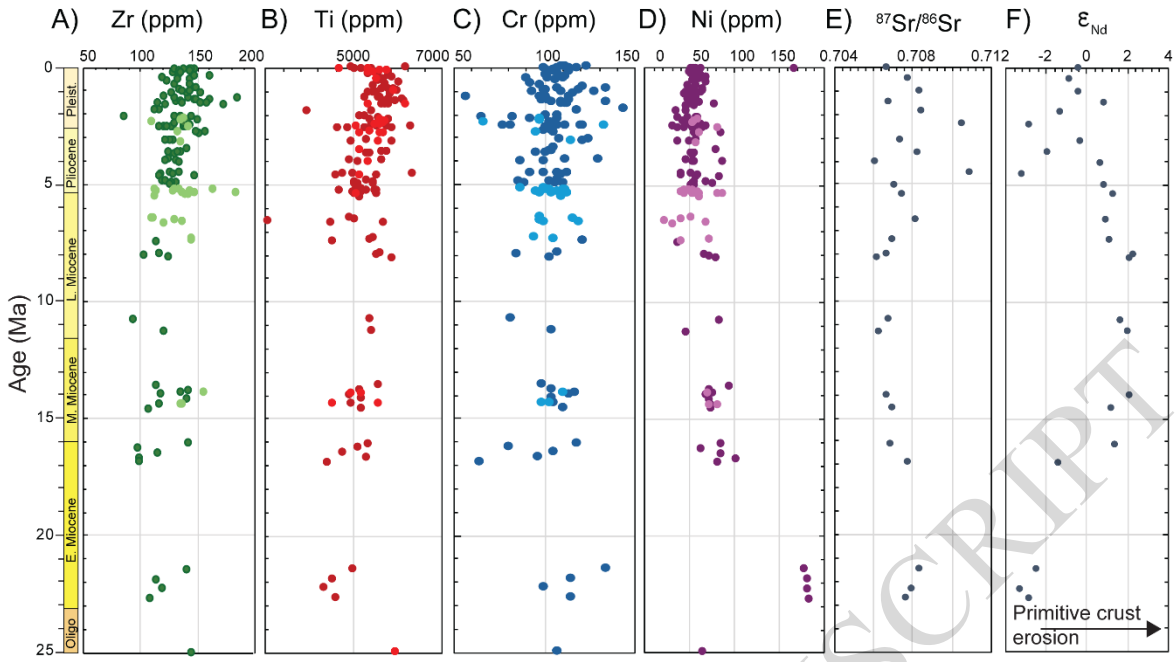


Figure 8

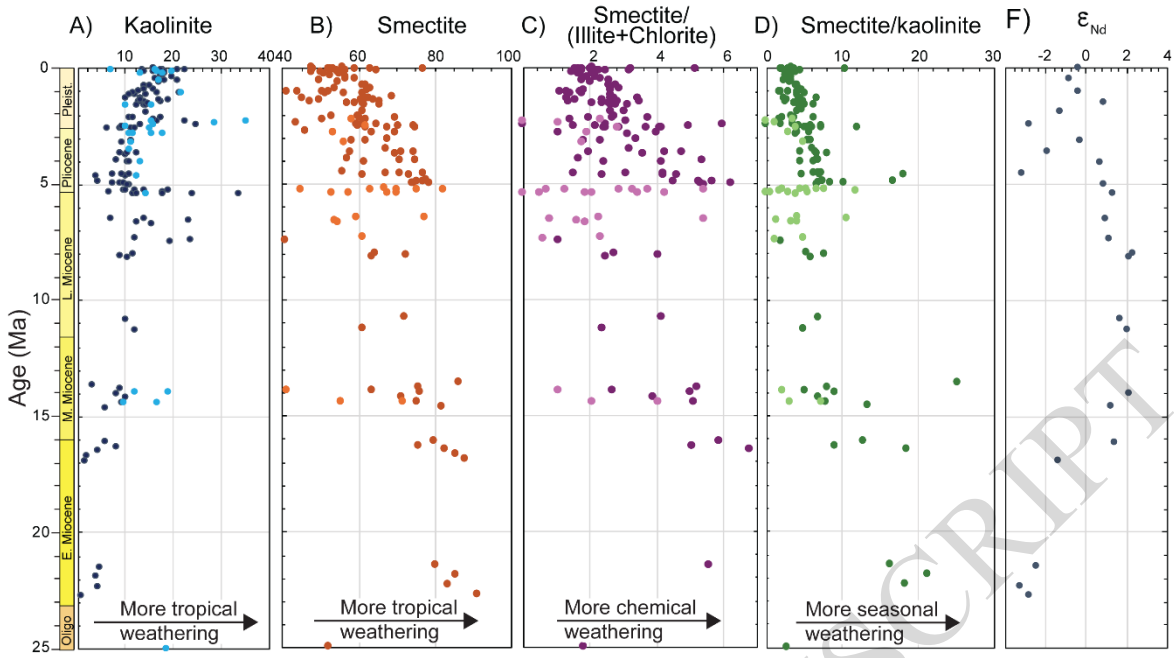


Figure 9

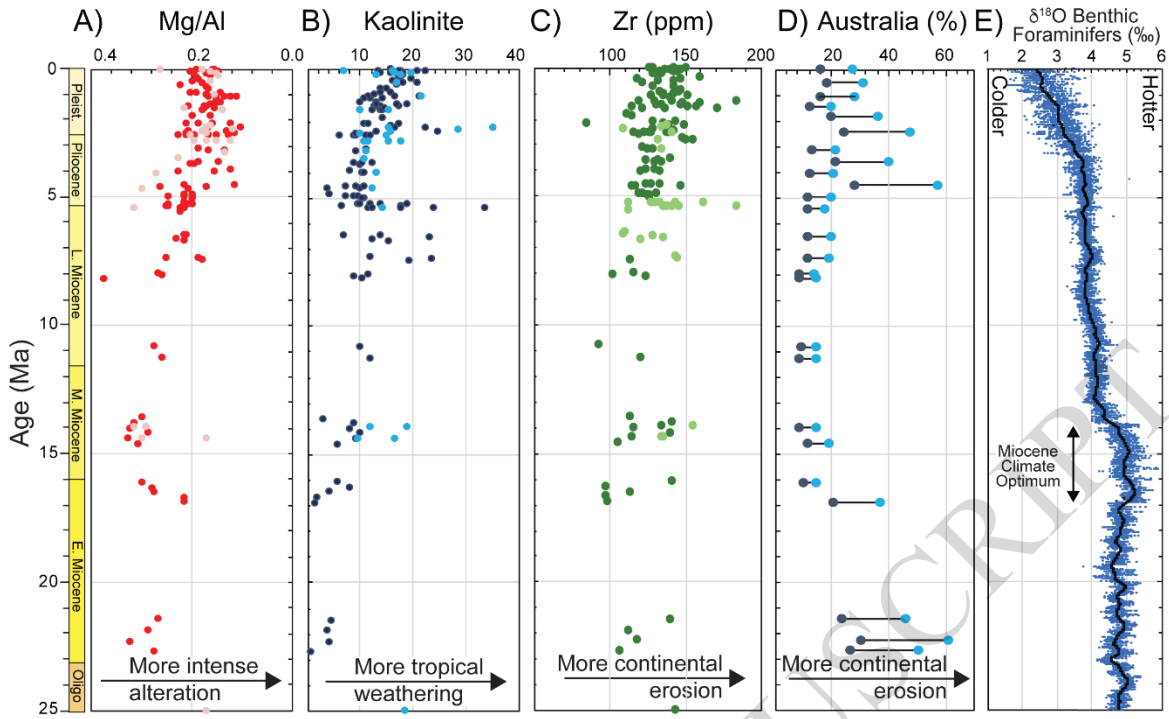


Figure 10

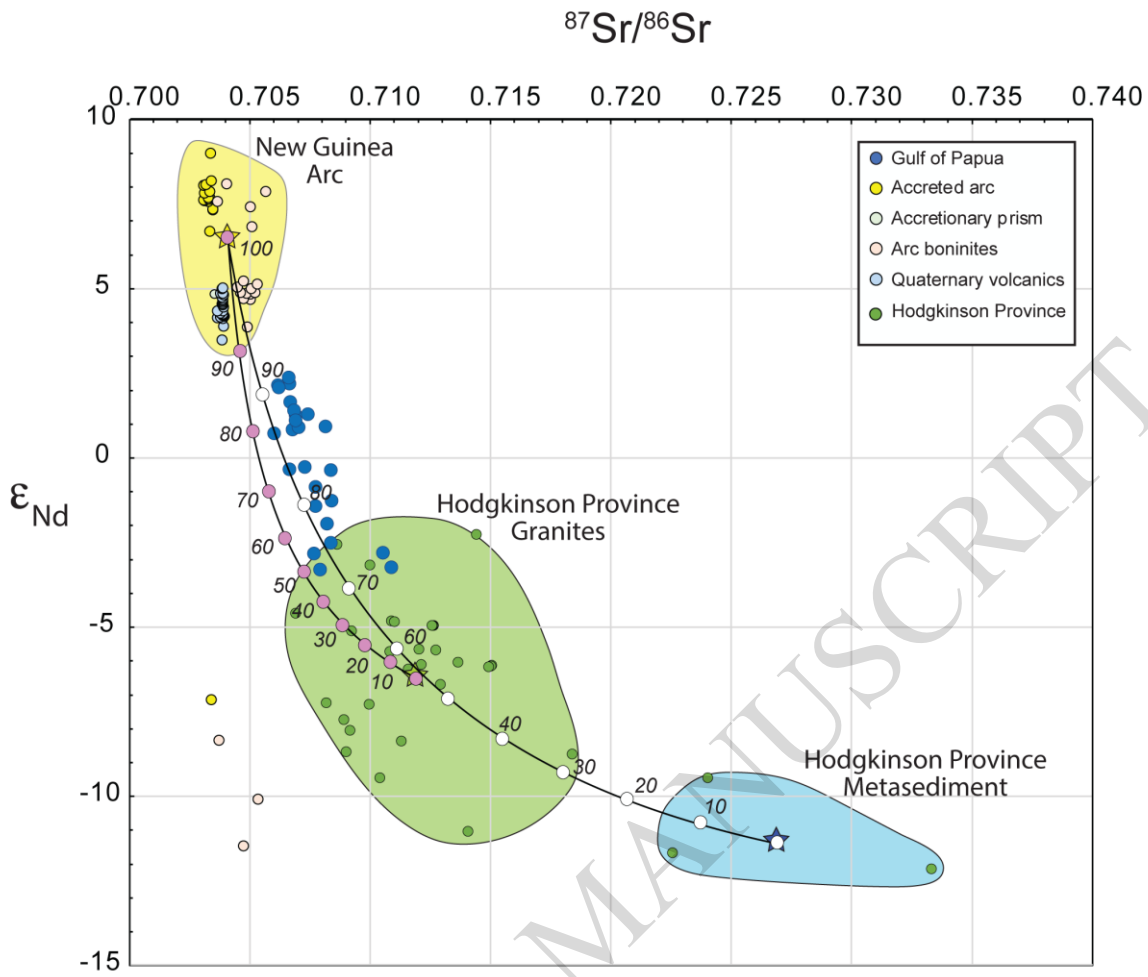


Figure 11

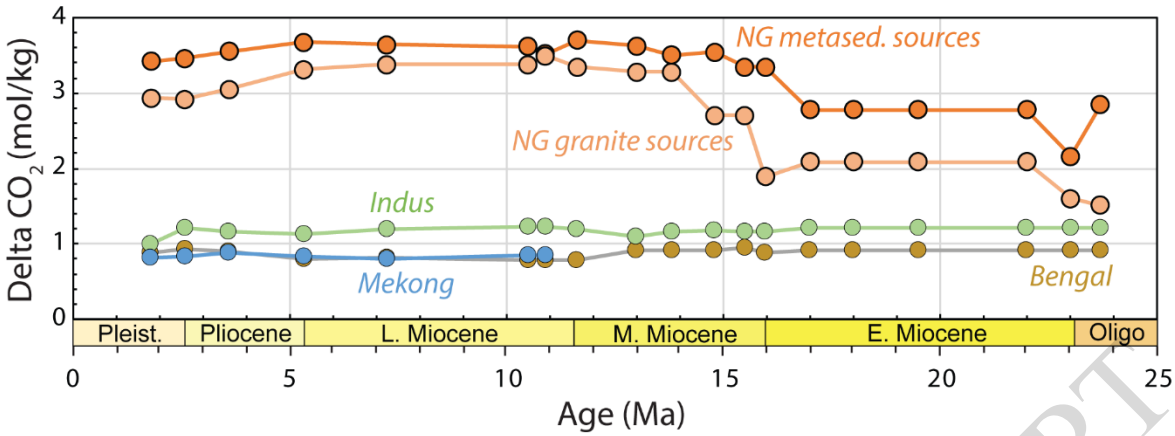


Figure 12

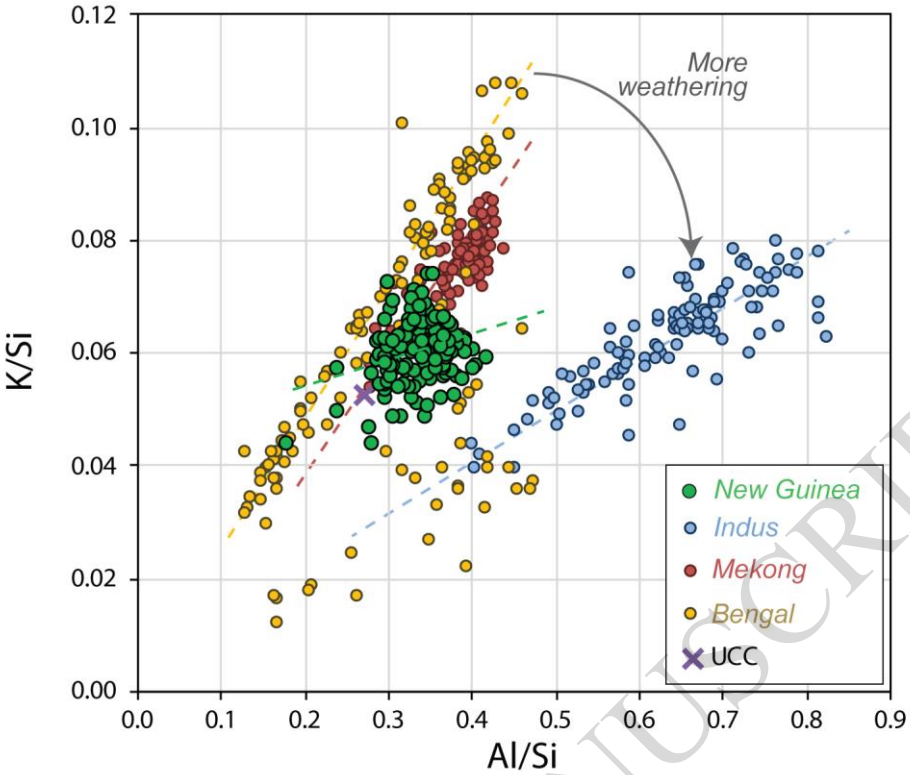


Figure 13

Table 1

| **Source region** | **Area ($km^2$)** | **Area %** |
|---|---|---|
| Fold and thrust belt (carbonate) | 20,850 | 15.2 |
| Quaternary volcanic rocks | 7,530 | 5.5 |
| Paleozoic basement | 2,060 | 1.5 |
| Ophiolite | 1,436 | 1.0 |
| Arc volcanics (Paleogene-Miocene) | 1,400 | 1.0 |
| Fold and thrust belt (siliciastic) | 37,320 | 27.3 |
| Jimi Kubor Terrane (Mesozoic sediment) | 12,660 | 9.2 |
| Neogene diorite | 262 | 0.2 |
| Cenozoic-Mesozoic metamorphic rocks | 13,616 | 9.9 |
| Aure Accretionary Prism | 27,170 | 19.8 |
| Cretaceous-Eocene oceanic basalts | 9,474 | 6.9 |
| Miocene volcanics and sediments | 3,100 | 2.3 |
| Total | 136,878 | |
| **Siliciclastic sources** | | |
| Continental rocks | 69,018 | 59.5 |
| Arc-ophiolite rocks | 47,010 | 40.5 |
| Total | 116,028 | |

Table 2

| DSDP Sample Number | Lab number | Depth (mbsf) | Age (Ma) | $^{87}Sr/^{86}Sr$ | 2SE |
|---|---|---|---|---|---|
| 210-1R-1-W (53-57) | 37 | 0.53 | 0.01 | 0.70667 | 0.00006 |
| 210-3R-2-W (117-120) | 40 | 20.67 | 0.48 | 0.70776 | 0.00012 |
| 210-6R-1-W (56-59) | 6 | 45.56 | 1.03 | 0.70839 | 0.00003 |
| 210-9R-4-W (27-30) | 8 | 76.77 | 1.46 | 0.70681 | 0.00005 |
| 210-11R-2-W (103-106) | 72 | 105.53 | 1.86 | 0.70844 | 0.00002 |
| 210-14R-2-W (120-123) | 79 | 161.20 | 2.41 | 0.71055 | 0.00003 |
| 210-19R-1-W (97-100) | 66 | 253.97 | 3.11 | 0.70733 | 0.00004 |
| 210-20R-1-W (104-107) | 49 | 273.04 | 3.62 | 0.70823 | 0.00005 |
| 210-21R-3-W (31-34) | 58 | 294.31 | 4.03 | 0.70605 | 0.00008 |
| 210-20R-1-W (104-107) | 54 | 310.36 | 4.53 | 0.71092 | 0.00007 |
| 210-23R-6-W (76-79) | 57 | 336.26 | 5.02 | 0.70707 | 0.00007 |
| 210-25R-4-W (80-83) | 141 | 370.30 | 5.42 | 0.70745 | 0.00007 |
| 210-27R-3-W (75-78) | 146 | 406.75 | 6.50 | 0.70818 | 0.00006 |
| 210-28R-4-W (108-111) | 132 | 426.58 | 7.34 | 0.70694 | 0.00010 |
| 210-29R-2-W (34-37) | 86 | 441.84 | 7.99 | 0.70664 | 0.00006 |
| 210-29R-4-W (131-134) | 84 | 445.81 | 8.15 | 0.70621 | 0.00005 |
| 210-30R-1-W (16-19) | 97 | 459.16 | 10.79 | 0.70672 | 0.00004 |
| 210-30R-2-W (67-70) | 90 | 461.17 | 11.28 | 0.70623 | 0.00003 |
| 210-31R-3-W (75-78) | 81 | 480.75 | 14.00 | 0.70667 | 0.00001 |
| 210-31R-6-W (78-81) | 91 | 485.28 | 14.59 | 0.70694 | 0.00001 |
| 210-32R-1-W (80-83) | 101 | 496.80 | 16.10 | 0.70688 | 0.00005 |
| 210-32R-5-W (80-83) | 96 | 502.80 | 16.89 | 0.70775 | 0.00003 |
| 210-33R-1-W (75-79) | 98 | 515.75 | 21.45 | 0.70839 | 0.00011 |
| 210-33R-3-W (82-85) | 87 | 518.82 | 22.30 | 0.70796 | 0.00011 |
| 210-33R-4-W (80-83) | 89 | 520.30 | 22.71 | 0.70770 | 0.00014 |

Table 3

| DSDP Sample number | Age (Ma) | Paleozoic Granite End Member % Australian Crust | Delta $CO_2$ (mol/kg) |
|---|---|---|---|
| 210-1R-1-W (53-57) | 0.01 | 28.0 | 3.399 |
| 210-3R-2-W (117-120) | 0.48 | 32.0 | 2.929 |
| 210-6R-1-W (56-59) | 1.03 | 29.0 | 2.782 |
| 210-9R-4-W (27-30) | 1.46 | 20.8 | 3.012 |
| 210-11R-2-W (103-106) | 1.86 | 37.0 | 2.845 |
| 210-14R-2-W (120-123) | 2.41 | 48.0 | 2.453 |
| 210-19R-1-W (97-100) | 3.11 | 22.0 | 3.377 |
| 210-20R-1-W (104-107) | 3.62 | 41.0 | 2.614 |
| 210-21R-3-W (31-34) | 4.03 | 21.0 | 3.436 |
| 210-22R-1-W (136-139) | 4.53 | 58.0 | 2.143 |
| 210-23R-6-W (76-79) | 5.02 | 20.5 | 3.419 |
| 210-25R-4-W (80-83) | 5.42 | 18.0 | 3.440 |
| 210-27R-3-W (75-78) | 6.50 | 20.2 | 3.296 |
| 210-28R-4-W (108-111) | 7.34 | 20.0 | 3.465 |
| 210-29R-2-W (34-37) | 7.99 | 14.7 | 3.466 |
| 210-29R-4-W (131-134) | 8.15 | 15.1 | 3.267 |
| 210-30R-1-W (16-19) | 10.79 | 15.4 | 3.377 |
| 210-30R-2-W (67-70) | 11.28 | 15.2 | 3.491 |
| 210-31R-3-W (75-78) | 14.00 | 15.0 | 3.377 |
| 210-31R-6-W (78-81) | 14.59 | 19.5 | 3.284 |
| 210-32R-1-W (80-83) | 16.10 | 15.5 | 3.280 |
| 210-32R-5-W (80-83) | 16.89 | 38.0 | 2.706 |
| 210-33R-1-W (75-79) | 21.45 | 47.0 | 1.887 |
| 210-33R-3-W (82-85) | 22.30 | 62.0 | 1.598 |
| 210-33R-4-W (80-83) | 22.71 | 51.0 | 1.508 |

Table 4

| | $SiO_2$ | $Al_2O_3$ | $Fe_2O_3$ | MgO | $TiO_2$ | CaO |
|---|---|---|---|---|---|---|
| New Guinea Arc | 52.36 | 11.75 | 2.89 | 14.35 | 0.58 | 7.17 |
| UCC | 66.62 | 15.40 | 5.04 | 2.48 | 0.64 | 3.59 |